*Clinical Science* (2019) **133** 1759–1777
https://doi.org/10.1042/CS20190672

PORTLAND PRESS

Research Article

# Mitochondrial ROS-induced lysosomal dysfunction impairs autophagic flux and contributes to M1 macrophage polarization in a diabetic condition

**Yujia Yuan[1], Younan Chen[1], Tianqing Peng[2,3], Lan Li[1], Wuzheng Zhu[1], Fei Liu[1], Shuyun Liu[1], Xingxing An[1], Ruixi Luo[1], Jingqiu Cheng[1], Jingping Liu[1,4] and Yanrong Lu[1]**

[1]Key Laboratory of Transplant Engineering and Immunology, NHFPC, and Regenerative Medicine Research Center, West China Hospital, Sichuan University, Chengdu, China; [2]Critical Illness Research, Lawson Health Research Institute, London Health Sciences Centre, London, Ontario, Canada; [3]Departments of Medicine and Pathology, University of Western Ontario, London, Ontario, Canada; [4]Center for Metabolic and Vascular Biology, School for Nutrition and Health Promotion, College of Health Solutions, Arizona State University, Scottsdale, AZ, USA

**Correspondence:** Yanrong Lu (luyanrong@scu.edu.cn) or Jingping Liu (liujingping@scu.edu.cn)



Macrophage polarization toward the M1 phenotype and its subsequent inflammatory response have been implicated in the progression of diabetic complications. Despite adverse consequences of autophagy impairment on macrophage inflammation, the regulation of macrophage autophagy under hyperglycemic conditions is incompletely understood. Here, we report that the autophagy–lysosome system and mitochondrial function are impaired in streptozotocin (STZ)-induced diabetic mice and high glucose (HG)-stimulated RAW 264.7 cells. Mitochondrial dysfunction promotes reactive oxygen species (ROS) production and blocks autophagic flux by impairing lysosome function in macrophages under hyperglycemic conditions. Conversely, inhibition of mitochondrial ROS by Mito-TEMPO prevents HG-induced M1 macrophage polarization, and its effect is offset by blocking autophagic flux. The role of mitochondrial ROS in lysosome dysfunction and M1 macrophage polarization is also demonstrated in mitochondrial complex I defective RAW 264.7 cells induced by silencing NADH:ubiquinone oxidoreductase subunit-S4 (Ndufs4). These findings prove that mitochondrial ROS plays a key role in promoting macrophage polarization to inflammatory phenotype by impairing autophagy–lysosome system, which might provide clue to a novel treatment for diabetic complications.

## Introduction

In the last several decades, the increased prevalence of diabetes and its associated complications have been a serious health problem worldwide [1,2]. Diabetic complications are commonly caused by chronic low-grade inflammation, which is characterized by elevated circulating pro-inflammatory cytokines, leukocyte activation markers, as well as increased macrophage infiltration into adipose, kidney, and other tissues [3–5]. Studies reported that hyperglycemia, a main symptom of diabetes, could induce macrophage polarization into the pro-inflammatory M1 phenotype with production of pro-inflammatory mediators such as interleukin-1β (IL-1β), interleukin-6 (IL-6), and tumor necrosis factor-α (TNF-α) [6], which contribute to the development of diabetic complications [7–9].

Oxidative stress seems to be an important executor of macrophage polarization to the M1 phenotype in obesity-associated insulin resistance [10,11], and it is well known that mitochondria are the primary source of reactive oxygen species (ROS) in macrophage polarization [12]. Elevated glucose induces excessive production of ROS and reactive nitrogen species (RNS), leading to pro-inflammatory activation of macrophages *in vitro* [9,13]. Moreover, systemic inflammation with a predominant M1 polarization, which can be attenuated by using a mitochondria-targeted antioxidant, Mito-TEMPO, is observed in

Received: 30 June 2019
Revised: 30 June 2019
Accepted: 02 August 2019

Accepted Manuscript Online: 05 August 2019
Version of Record published: 14 August 2019

*Clinical Science* (2019) **133** 1759–1777
https://doi.org/10.1042/CS20190672

Ndufs4$^{-/-}$ (a critical component of mitochondrial complex I) mice. This supports a key role for mitochondrial ROS in macrophage polarization into the M1 phenotype [14].

Autophagy is one of the major cellular degradation pathways in many aspects of cell homeostasis. Its process comprises 2 stages: the early stage and the late stage. The early stage includes the formation of phagophores, the precursor to autophagosomes which capture damaged cellular molecules and organelles; the late stage is responsible for the digestion of entrapped components within the autolysosome formed by the fusion of an autophagosome and lysosome [15]. Recent studies have shown that impaired or deficient macrophage autophagy promoted macrophage polarization into the pro-inflammatory M1 phenotype, which could cause hepatic inflammation, fibrosis and insulin resistance [16,17]. Conversely, restoration of autophagy in macrophages improves cardiac homeostasis in high-fat diet-induced obese mice [18]. These studies indicated a potential protective role of macrophage autophagy in metabolic disorders. However, the effect of diabetes on the autophagy process in macrophages is not completely clear.

Lysosome function is essential for maintaining normal autophagic flux. Lysosomes are acidic organelles containing a wide spectrum of hydrolytic enzymes, including proteases, peptidases, phosphatases, nucleases, glycosidases, sulfatases, and lipases, which are designated for all types of macromolecules. A recent study demonstrated that high-fat diet-induced lysosomal dysfunction and impaired autophagic flux of proximal tubular cells (PTCs) contributed to lipotoxicity in the kidney [19]. In addition, the activity of lysosomal enzymes in the liver was decreased in a streptozotocin (STZ)-induced diabetic rat model, suggesting that hyperglycemia may induce lysosomal impairment in diabetes mellitus (DM) [20]. Moreover, the presence of excess glucose inhibited lysosomal function in macrophages [21]. Given the essential role of lysosomes in the maturation/degradation stage of autophagy, it is possible that progressive dysfunction in the lysosomal apparatus is deleterious to macrophages. Importantly, mitochondrial dysfunction induced by genetic ablation of mitochondrial proteins or by chemical inhibition of the electron transport chain impaired lysosomal structure and activity in neuronal cells and T cell, which leading to neurodegeneration and an inflammatory T cell response [22,23]. However, the involvement of mitochondrial dysfunction in autophagy–lysosome impairment and macrophage polarization in diabetes remains unknown.

In the present study, we demonstrate that mitochondrial ROS derived from damaged mitochondria promotes macrophage polarization toward the M1 phenotype expressing high levels of CD11c and iNOS-1 in diabetes. This process is mediated by impairing lysosomal function and autophagic flux.

# Materials and methods

## Reagents and antibodies

Glucose (G8270), Mannitol (78513), and STZ (S0130) were purchased from Sigma. HCQ (HY-B1370) and CCCP (HY-100941) were purchased from MedChemExpress. Mito-TEMPO (sc-221945) was purchased from Santa Cruz Biotech. The trizol reagent (15596026) was purchased from Invitrogen, and SYBR Green PCR master mix kit (1725201) was obtained from Bio-Rad Laboratories. ELISA kits for mouse MCP-1 (EMC113), and mouse IL-1β (EMC001b) were obtained from Neobioscience. JC-1 probe (22200) was from AAT Bioquest. Mito-tracker-green (C1048), lyso-tracker-red (C1046), DCFA-DH (S0033), ATP assay kit (S0026), NAC (S0077) and Catalase Assay Kit (S0051) were from Beyotime. MitoSOX™ Red (M36008) and LysoSensor™ Yellow/Blue DND-160 (L7545) were purchased from Thermo Fisher. RFP-GFP-LC3 Adenovirus was purchased from Hanbio Biotechnology. Different antibodies like CD206 (ab64693), MFN2 (ab50838), DRP1 (ab156951), PGC-1α (ab54481), MCP-1 (ab25124), LAMP1 (ab24170), Ubiquitin (ab7254), P62 (ab109012), PINK1 (ab23707), and PARKIN (ab77924) were purchased from Abcam. SIRT3 (A5718) was obtained from Abclonal. iNOS-1 (D6B6S), IL-1β (31202), CTSB (D1C7Y), BECN1 (D40C5), ATG5 (D5F5U), and LC3B (2775) were purchased from Cell Signaling Technology.

## Animal models

All mice were housed in the animal center of West China Hospital, Sichuan University in accordance with the Guide for the Care and Use of Laboratory Animals. All experimental procedures were approved by the Animal Use Subcommittee at Sichuan University, China. Male BALB/c mice (6–8-week-old) were randomized into the following two groups: (i) a normal control (NC) group ($n$=6) and (ii) a DM group ($n$=24). Diabetes was induced by an intraperitoneal injection of streptozotocin (STZ) (Sigma, 150 mg/kg, dissolved in 0.1 mol/L sodium citrate, pH 4.5), and the diagnostic criteria for DM are based on a fasting blood glucose level ≥ 16.7 mmol/L.

## Cell culture

A mouse monocytic cell line, RAW 264.7, was obtained from ATCC and maintained in 1640 media with 10% heat-inactivated FBS, 100 U/ml penicillin and 100 mg/ml streptomycin.

**Table 1 Primers used for qPCR analysis**

| | | | |
|---|---|---|---|
| iNOS-F | CAGCTGGGCTGTACAAACCTT | ND1-F | CAAACCTCCTATCAGCCATCC |
| iNOS-R | CATTGGAAGTGAAGCGTTTCG | ND1-R | AGCGAAGAATCGGGTCAAG |
| Arg-1-F | AGACAGCAGAGGAGGTGAAGAG | CO1-F | TCTAATCGCCATAGCCTTCC |
| Arg-1-R | CGAAGCAAGCCAAGGTTAAAGC | CO1-R | GCGTCTGCAAATGGTTGTAA |
| CD206-F | GGATTGTGGAGCAGATGGAAG | ATP6-F | CTCACTTGCCCACTTCCTTC |
| CD206-R | CTTGAATGGAAATGCACAGA | ATP6-R | GTAAGCCGGACTGCTAATGC |
| ATP5B-F | TTTGCTGGTGTTGGTGAGAG | Cytb -F | CAAACCTCCTATCAGCCATCC |
| ATP5B-R | GGTGGTTCGTTCATCTGTCC | Cytb -R | AGCGAAGAATCGGGTCAAG |
| COX5b-F | CAGAAGGGACTGGACCCATA | ACTIN-F | AAGGCCAACCGTGAAAAGAT |
| COX5b-R | TTCACAGATGCAGCCCACTA | ACTIN-R | GTGGTACGACCAGAGGCATAC |
| SDHD-F | TGTCACCAAGCCACCACTC | | |
| SDHD-R | CCACAGAGCAGGGATTCAAG | | |

## Isolation of peritoneal macrophages

Peritoneal macrophages were collected from the mice by infusing their peritoneal cavity with 10 ml ice-cold phosphate buffered saline (PBS). The collected cells were centrifuged and the cell pellets re-suspended in 1640 medium with 10% fetal bovine serum. One hour after incubation under 5% $CO_2$ in a humidified incubator, non-adherent cells were removed by washing with PBS once at 37°C. Adherent macrophages were cultured in 1640 medium with 10% fetal bovine serum.

## Analysis of macrophages phenotype by flow cytometry

Flow cytometric identification was executed using combinations of the following mAbs: F4/80-APC (123116, Biolegend), CD206-PE (141706, Biolegend), and CD11c-FITC (N418, Miltenyi Biotec). After incubation for 30 min at 37°C, flow cytometry analysis was performed on the FACSCalibur instrument (BD Biosciences) equipped with Cell Quest software.

## Real-time PCR quantification

Total RNA was extracted from cells with trizol, and then reverse-transcribed to cDNA using a transcriptor first-stand cDNA synthesis kit and random primers. Quantitative real-time PCR (qPCR) was performed in triplicates using a Chromo4 cycler (Bio-Rad) and SYBR Green PCR master mix kit with specific primers (Table 1). Data analysis was performed using the $\Delta\Delta C_t$ method.

## Silencing of *Ndufs4 and Atg5* siRNA

The siRNAs for *Atg5* (sense, 5′-GCAUUAUCCAAUUGGUUUATT-3′; antisense, 5′-UAAACCAAUUGG AUAAUGCTT-3′) were purchased from GenePharma (Shanghai, China), and *Ndufs4* RNAi (sense, 5′-CCAGAAAGGUCAGAAUCUUdTdT-3′; antisense, 5′- GGUCUUUCCAGUCUUAGAAdTdT-3′) were purchased from Ribobio Co., Ltd, (Guangzhou, China). For the interference for *Atg5* and *Ndufs4,* RAW 264.7 cells were transfected with 50 nM siRNA by Lipofectamine 2000 (11668019, Thermo Fisher), respectively, and after 48 h, gene silencing was proved by analysis of protein expression using Western blotting.

## ELISA detection

The soluble cytokines including TNF-α, and MCP-1 in culture media and sera of mice were assayed using commercially available ELISA detection kits (EMC102a and EMC113, Neobioscience, China), according to the manufacturer's instructions.

## Western blot analysis

Cells were homogenized in RIPA lysis buffer containing PMSF. Proteins were collected by centrifuging at 12000 rpm at 4°C, and then boiled for 10 min. Briefly, equal amounts of proteins were separated on sodium dodecyl sulfate-polyacrylamide gel electrophoresis (SDS-PAGE) and transferred to nitrocellulose membranes, followed by incubation with appropriate primary and secondary antibodies. Blots were visualized by Immobilon™ Western Chemiluminescent HRP Substrate.

*Clinical Science* (2019) **133** 1759–1777
https://doi.org/10.1042/CS20190672

## Quantification of mitochondrial morphology

RAW 264.7 cells were seeded and grown on glass coverslips (MatTek Corporation). After incubating the cells with Mito-Tracker Green at 37°C for 30 min, mitochondrial morphology was visualized and images were acquired using LSM-800 time-lapse confocal microscopy with an 100 × oil immersion objective lens. Z-stacks of thresholder images were volume-reconstituted using the Volume J plug-in. Twenty cells were analyzed in each sample to determine cells undergoing mitochondrial fragmentation. A decrease in mitochondrial length was considered as mitochondrial fission, and quantified by Image-Pro Plus 6.0 software.

## CCK-8 assay

Cell viability was assessed by the cell counting kit 8 (CCK-8) assay. Cells were seeded in 96-well plates, and each plate contained $1 \times 10^4$ cells. After treatment, CCK8 solution was added into the cells and quantified by an enzyme-linked immunosorbent assay microplate reader (BioTek, U.S.A.) at 450 nm. The OD of the results was indicated as a percentage of cell viability related to the control group.

## ROS detection

The ROS generation in macrophages was evaluated according to the fluorescence intensity of DCFA-DH or MitoSOX™ Red. Cells were incubated with 1640 medium containing probes for 30 min at 37°C in the dark. After rinsing, the fluorescent signals of labeling ROS formation were immediately measured via a fluorescence microscope.

## Measurement of mitochondrial membrane potential ($\Delta\psi$ m)

$\Delta\psi$ was determined using a dual-emission, potential-sensitive, and fluorescent probe, JC-1, which exhibits potential-dependent accumulation in mitochondria, indicated by a fluorescence emission shift from green (530 nm) to red (590 nm). Briefly, cells were incubated with 5 nM of JC-1 for 30 min at 37°C and then analyzed by flow cytometry. Mitochondrial polarization is indicated by an increase in the red/green fluorescence intensity ratio.

## ATP measurement

Intracellular ATP levels were measured using a commercially available intracellular ATP measurement kit (Beyotime Biotechnology, China) according to the manufacturer's instructions. Briefly, the collected cells and tissues were lysed with a lysis buffer and then centrifuged at 12000 ***g*** for 10 min at 4°C. After that, an aliquot of the supernatant plus an ATP detection solution was added to a 96-well plate (Corning, NY, U.S.A.). Luminescence was detected using a SpectraMax M5 MultiMode Microplate Reader. The ATP level was presented as nanomoles per milligram of protein.

## Immunofluorescence

After treatments, RAW 264.7 cells were incubated with MitoTracker Deep Red (100 nM) for 30 min at 37°C, fixed in 4% paraformaldehyde, and permeabilized with 0.1% Triton X-100 by blocking with 1% bovine serum albumin (BSA, A7030, Sigma–Aldrich). Then, the cells were immunolabeled with primary antibodies (Ubiquitin at 1:200 ratio, or Lamp1 at 1:400 ratio) overnight at 4°C. After washing, the cells were incubated with a corresponding FITC-conjugated secondary antibody (1:400) in 1% BSA for 1 h at 37°C. Nuclei were stained with DAPI (D9542, Sigma–Aldrich) for 5 min at room temperature. The fluorescent signals were examined using a confocal laser scanning microscope, and the overlap coefficient was analyzed by Image Plus 6.0.

## GFP-RFP-LC3 analysis

To evaluate the numbers of autophagosomes and autolysosomes, mGFP-RFP-LC3 adenovirus was used. Differentiated RAW 264.7 were transduced with mGFP-RFP-LC3 adenovirus for 24 h followed by exposure to a HG medium for 48 h. After treatment, cells were counter-stained for nuclei using Hoechst (62249; Thermo Fisher Scientific) for 10 min. Then, cells were imaged at excitation/emission maxima of approximately 504/511 nm for GFP and 555/584 nm for RFP under fluorescence microscope. All samples were examined under a Zeiss confocal laser scanning microscope (Zeiss, LSM 780) equipped with a 100 × oil immersion objective.

## Quantity of lysosome

To monitor pH-sensitive indices of lysosomal function, cells were collected and washed with PBS twice. Then, cells were incubated with 100 nM of lysotracker red at 37°C for 0.5 h. After incubation, cells were collected and determined using a flow cytometer or fluorescence microscope. LysoTracker intensity relative to the baseline suggests the integrity, or quantity of lysosomal function, when compared with the control.

## Lysosomal pH measurement

To determine lysosomal pH more accurately, LysoSensor yellow/blue DND-160 was used in the experience. Cells were collected and incubated with the probe at a concentration of 1 mg/ml for 5 min at 37°C. The LysoSensor dye is a ratiometric probe that produces yellow fluorescence in acidic environments but changes to blue fluorescence in neutral environments. After incubation, cells were read using a SpectraMax M5 MultiMode Microplate Reader. Cells were excited with 365 nM, and 485/535 nm was then calculated for each sample.

## Statistical analysis

Results are expressed as the means ± SEM from at least three independent experiments. Statistical analysis was performed by one-way ANOVA tests with Tukey's post hoc analyses using SPSS version 17.0 (SPSS Inc.). A $P$ value $< 0.05$ is considered as a statistical difference.

# Results

## Diabetes promotes macrophage polarization to a pro-inflammatory phenotype

Flow cytometry analysis of peritoneal macrophages in STZ-induced diabetic mice showed that the proportion of M1 macrophages (CD206−CD11c+) was significantly increased, whereas the proportion of M2 macrophages (CD206+CD11c−) was significantly decreased when compared with non-diabetic mice (Figure 1A). Consistently, the mRNA and protein levels of the M1 biomarker iNOS-1 in peritoneal macrophages were markedly elevated starting from the second week post STZ injection (Figure 1B,C). In contrast, the mRNA and protein levels of M2 biomarkers CD206 and ARG-1 were slightly increased after 2 weeks of STZ injections but decreased after 4 weeks of STZ injection (Figure 1B,C). In line with macrophage polarization toward the M1 phenotype, the levels of pro-inflammatory cytokines (MCP-1 and IL-1β) in serum were higher in diabetic mice than in non-diabetic mice starting at 4 weeks after STZ injection (Figure 1D). Similarly, the protein levels of MCP-1 and IL-1β were increased in isolated macrophages of diabetic mice compared with non-diabetic mice (Figure 1E) These results demonstrated that diabetes facilitates M1 macrophage differentiation and suppresses M2 macrophage activation.

## Mitochondrial dysfunction increases mitochondrial ROS in macrophages under a diabetic condition

In diabetic mice, the mitochondrial fission protein dynamin-related protein 1 (DRP-1) was increased, suggesting that hyperglycemia induces mitochondrial fragmentation (Figure 2A). Meanwhile, diabetes caused a reduction of mitochondrial biogenesis-associated proteins including SIRT1, SIRT3, phosphorylated AMPK, and PGC-1α (Figure 2B). Diabetes also caused a reduction in mRNA expression of mtDNA-encoded subunits of mitochondrial complexes I, III, IV, and V and nuclear-encoded subunits in peritoneal macrophages of diabetic mice (Supplementary Figure S1). Consequently, the ATP and mitochondrial membrane potential ($\Delta\psi$ m) were reduced in macrophages of diabetic mice (Figure 2C,D). These abnormalities of mitochondria were correlated with an increase in mitochondrial ROS in peritoneal macrophages of diabetic mice in a time-dependent manner (Figure 2E). To investigate the change of mitochondrial dynamics in polarized macrophages from diabetic mice, we isolated M1- and M2-like macrophages. Confocal microscopy revealed that M1-like macrophages predominantly exhibited punctate mitochondria, and the mitochondrial length was shorter than M2-like macrophages (Figure 2F). Consistent with the observation of mitochondrial fragmentation, the protein level of mitochondrial fusion protein mitofusin-2 (MFN-2) in M1 macrophages was decreased, while mitochondrial fission protein DRP-1 was remarkably increased (Figure 2G). In addition, comparing with the M2-like macrophages, the ATP content in M1-like macrophages was reduced, and the mitochondrial ROS was increased (Figure 2H,I). These results suggested that diabetes-induced mitochondrial dysfunction and ROS production in macrophages may start from an early stage of diabetes, which is correlated with macrophage polarization.

To evaluate mitochondrial dysfunction *in vitro*, we incubated RAW 264.7 cells in high glucose (HG, 30 mM). Similar to the *in vivo* findings, when compared with control cells, HG-treated cells displayed smaller and punctate mitochondria with a significantly shorter length, suggesting that a HG environment induces mitochondrial fragmentation (Figure 3A). In addition, after HG treatment the protein level of DRP-1 was significantly increased in RAW 264.7 whole-cell lysates and mitochondrial fractions (Figure 3B). Meanwhile, a HG environment impaired $\Delta\psi$ m and decreased ATP production (Figure 3C,D). Consistently, mitochondrial dysfunction was associated with an increase

*Clinical Science* (2019) **133** 1759–1777
https://doi.org/10.1042/CS20190672

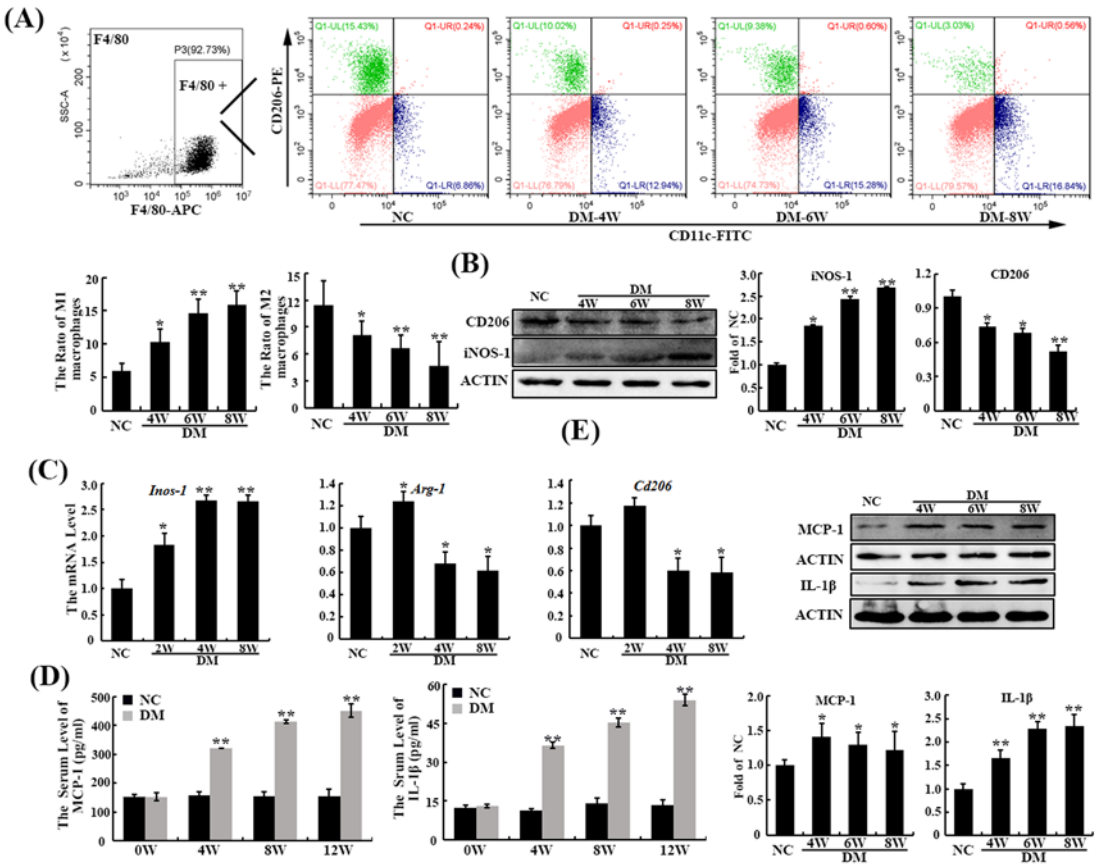


**Figure 1. Hyperglycemia induced inflammatory macrophages in STZ-induced diabetic mice**

(**A**) Peritoneal macrophages were harvested by lavage from diabetic mice at 4, 6, and 8 week post STZ injection, and the phenotype (M1: CD206−CD11c+; M2: CD206+CD11c−) was characterized by flow cytometry ($n$=4). (**B**) Representative images of WB and quantitative analyses of iNOS-1 and CD206 ($n$=4). (**C**) The abundance of M1 type marker (*Inos-1*) and M2 type markers (*Arg-1* and *Cd206*) were determined by qPCR. (**D**) The serum level of pro-inflammatory factors (MCP-1 and IL-1β) were measured by ELISA kits ($n$=5). (**E**) The expression of inflammatory proteins in macrophages isolated from diabetic mice was detected by WB ($n$=4). Data are provided as mean ± SEM. Statistically significant differences (*$P$<0.05, **$P$<0.01 vs. NC) are indicated.

in mitochondrial ROS production in HG-stimulated RAW 264.7 cells (Figure 3E,F), which could be abolished by a selective inhibitor of mitochondrial ROS, Mito-TEMPO.

## Blocking mitochondrial ROS inhibits RAW 264.7 polarizing toward the M1 phenotype in a diabetic condition

Flow cytometry analysis revealed that the percentage of M1 macrophages (CD206−CD11c+) was much higher in HG-stimulated RAW 264.7 cells when compared with NC (Figure 4A). This was supported by increased iNOS-1 and decreased CD206 levels in HG-incubated RAW 264.7 cells (Figure 4B,C). Furthermore, the protein levels of pro-inflammatory cytokines including IL-1β and MCP-1 were elevated in RAW 264.7 cells treated with HG (Figure 4B,C), and incubation in a HG environment for 48 h significantly increased the levels of IL-1β and MCP-1 secreted by RAW 264.7 cells (Figure 4D,E). By contrast, the M1 polarization of macrophages induced by HG was reversed by selective inhibition of ROS using Mito-TEMPO (Figure 4A–E). Moreover, to further strength the role of ROS on macrophage polarization, an independent pharmacological agent NAC was also used to quenching ROS, and similar effects were observed in NAC-treated groups.

The role of mitochondrial ROS in macrophage polarization to M1 phenotype was also determined by the *Ndufs4*-knockdown model. Ndufs4 is a critical protein for mitochondrial Complex I (C-I) assembly, and the silencing of *Ndufs4* by siRNA led to accumulation of mitochondrial ROS in RAW 264.7 cells (Figure 5A,B). Meanwhile, silencing *Ndufs4* promoted M1 polarization of macrophages as indicated by flow cytometry analysis (Figure 5C),

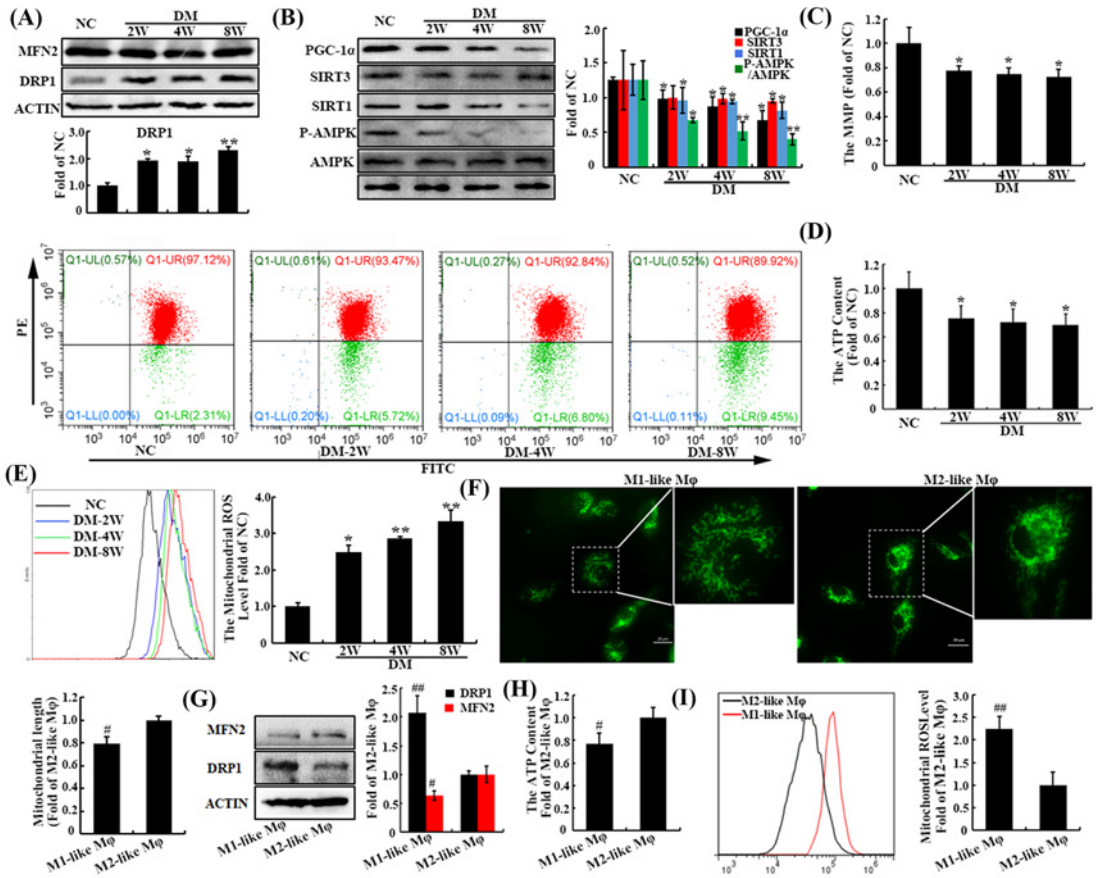


**Figure 2. Mitochondrial quality of macrophages in diabetic mice**

(**A**) Immunoblot quantification of DRP1 and MFN2 in macrophages of diabetic mice at 8th week post STZ injection ($n$=4). (**B**) Immunoblot analysis of mitochondrial biogenesis-related proteins (PGC-1α, SIRT1, SIRT3, P-AMPK, and AMPK) in macrophages from diabetic mice ($n$=3). (**C**) Quantitative analysis of mitochondrial membrane potential (Δψ m) was measured by JC-1 (37°C for 30 min) ($n$=3). (**D**) ATP content in macrophages was assessed using an ATP Assay Kit, and the data were represented as the rate of NC ($n$=5). (**E**) The mitochondrial ROS level of macrophages in mice. (**F**) Representative immunofluorescence of mitochondrial morphology in isolated M1-like and M2-like macrophages (M1-like Mϕ and M2-like Mϕ), loaded with Mito-tracker-green (100 nM), and the mitochondrial length was calculated using Image J ($n$=5). (**G**) Immunoblot quantification of DRP1 and MFN2 in isolated M1-like and M2-like macrophages ($n$=3). (**H and I**) ATP content and mitochondrial ROS in polarized macrophages from diabetic mice ($n$=4). Data are provided as mean ± SEM. Statistically significant differences (*$P$<0.05, **$P$<0.01 vs. NC group; $^{\#}P$<0.05, $^{\#\#}P$<0.01 vs. M2-like Mϕ group) are indicated.

increased iNOS-1, reduced CD206 protein, and elevated pro-inflammatory cytokines (IL-1β and MCP-1). These adverse effects were prevented by Mito-TEMPO (Figure 5D,E). To further demonstrate the role of ROS in macrophage polarization, we treated primary macrophages with $H_2O_2$ or tBHP. Similarly, inhibition of ROS by Mito-TEMPO reduced IL-1β, MCP-1, and iNOS-1 levels while increasing the expression of CD206 in macrophages treated with $H_2O_2$ or tBHP (Supplementary Figure S2). Taken together, these results suggest that ROS plays a key role in macrophage polarization under diabetic conditions.

## Lysosome function and autophagosome clearance are impaired in macrophages under diabetic conditions

We next analyzed the effect of ROS on autophagy in macrophages of diabetic mice. The protein levels of microtubule-associated protein 1 light chain 3 II (LC3II) increased at 4 weeks and sequentially reduced at 6 and 8 weeks in macrophages of diabetic mice (Figure 6A). In addition, the expression of BECN1 and autophagy related 5 (ATG5), which were positively correlated with autophagosome synthesis, were not changed at 4 weeks but

*Clinical Science* (2019) **133** 1759–1777
https://doi.org/10.1042/CS20190672

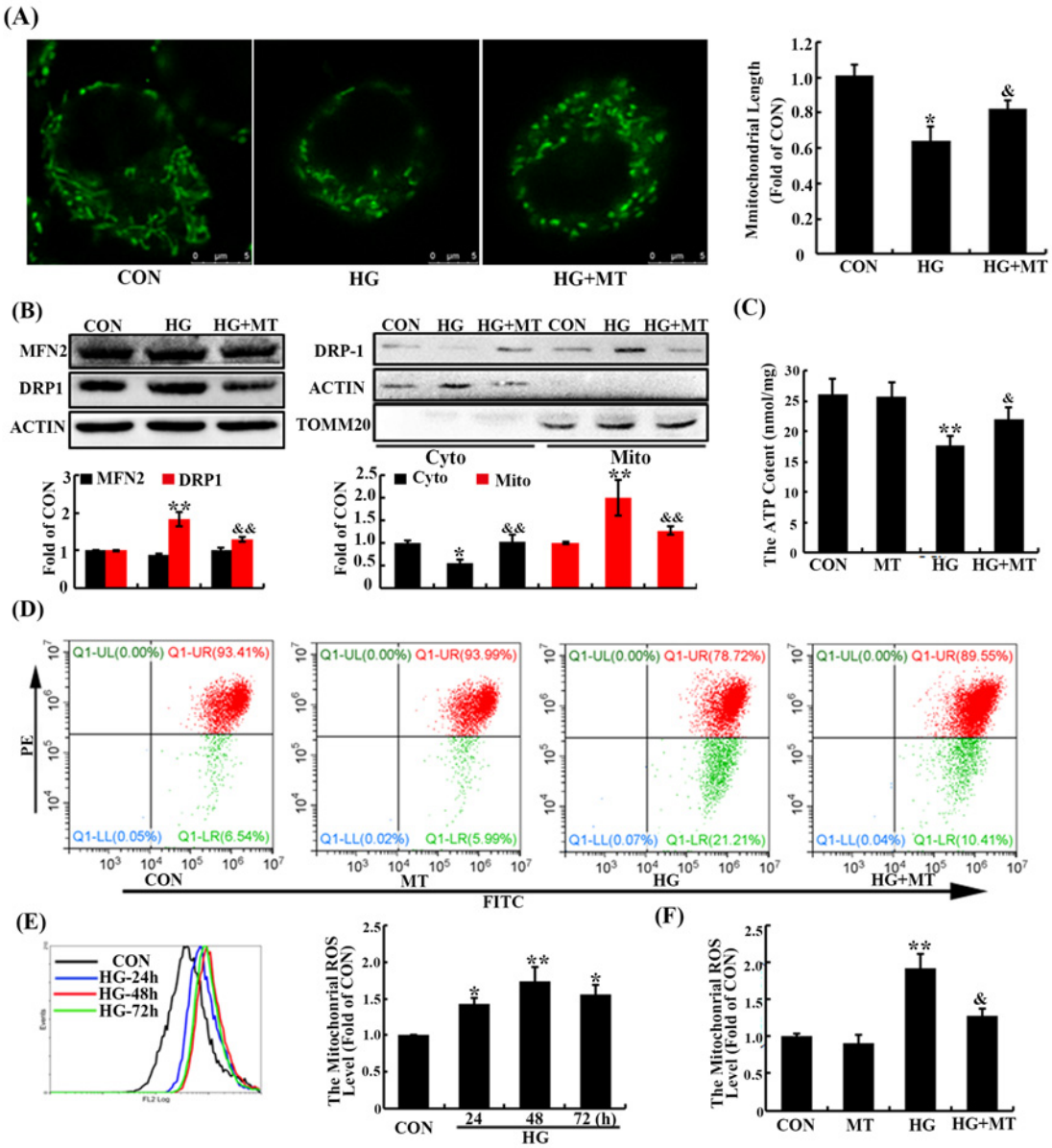


**Figure 3. Changes in mitochondrial network in HG-induced RAW 264.7 cells**

Cells were treated with high glucose (HG, 30 mM) for 48 h in the presence or absence of Mito-TEMPO (MT, 50 nM). (**A**) Representative immunofluorescence and quantify of mitochondrial morphology in RAW 264.7 cells ($n$=5). (**B**) Immunoblot quantification of DRP-1 in mitochondrial and cytosolic fractions in RAW 264.7 cells ($n$=3). (**C**) The ATP content in RAW 264.7 cells, and the data were represented as the rate of control ($n$=4). (**D–F**) The mitochondrial membrane potential ($\Delta\psi$ m) and mitochondrial ROS were measured by flow cytometry ($n$=4). Data are provided as mean ± SEM. Statistically significant differences (*$P$<0.05, **$P$<0.01 vs. CON group; $^{\&}P$<0.05 vs. HG group) are indicated.

were reduced at 6 and 8 weeks in the macrophages of diabetic mice (Figure 6A). In contrast, an SQSTM1 (P62, an ubiquitin-binding protein delivered to lysosomes for degradation) protein was increased in the macrophages of diabetic mice in a time-dependent manner (Figure 6A), suggesting impaired autophagosome clearance in macrophages at the early stage of diabetes. These results also indicated that diabetes might impair lysosomal function in macrophages. This hypothesis was supported by a time-dependent loss of LysoTracker-red intensity in macrophages starting from 4 weeks after STZ injection (Figure 6B). Moreover, diabetes increased the pH value of lysosomes in macrophages (Figure 6C). The protein levels of LAMP1 and the endopeptidase cathepsin B (CTSB) were decreased in the macrophages of diabetic mice starting 4 weeks after the STZ injection, which were associated with reduced

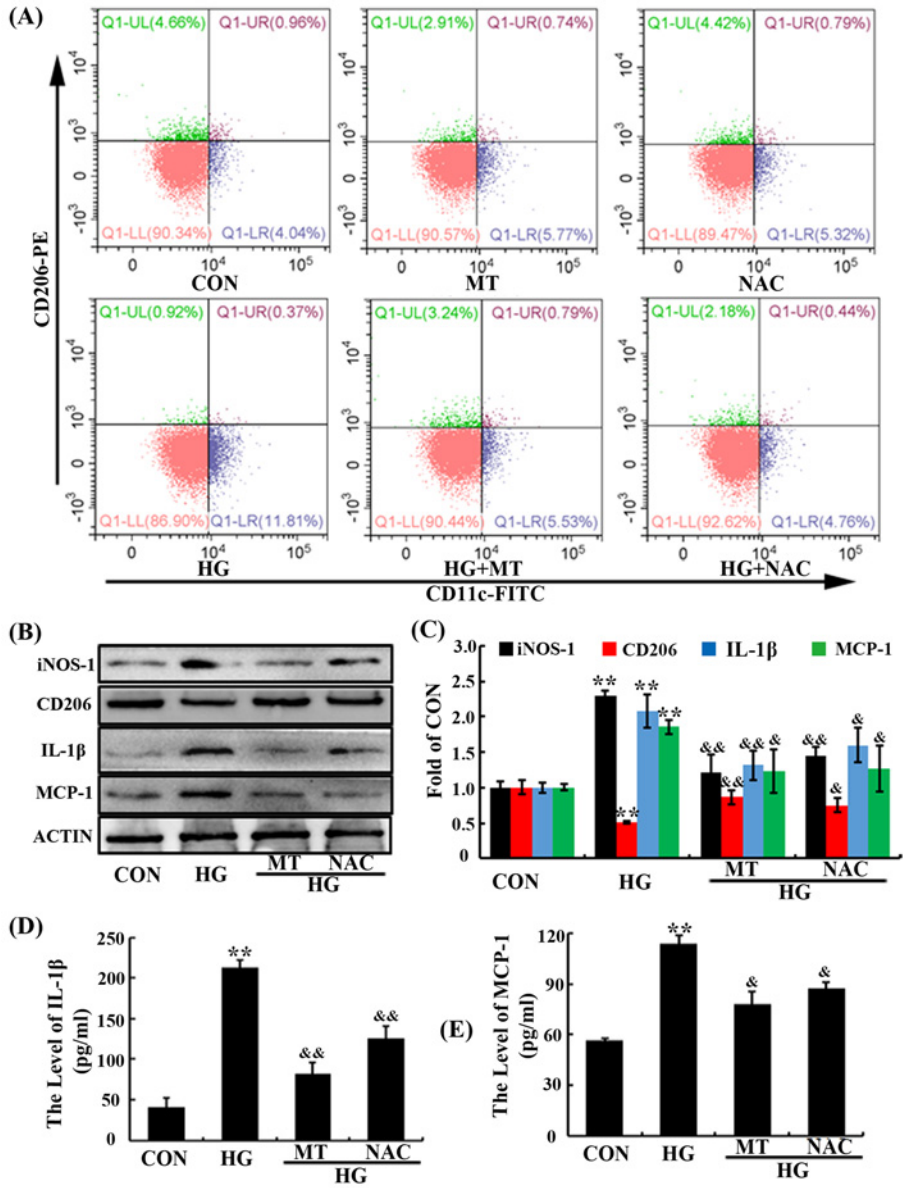


**Figure 4. Inhibition of ROS promotes RAW 264.7 to polarize toward M2 phenotype under HG stimuli**

Cells were preincubated with ROS inhibitors Mito-TEMPO (MT, 50 nM) or NAC (10 mM) and then treated with HG for 48 h. (**A–C**) Analysis of polarized phenotype in HG-induced RAW 264.7 cells with MT or NAC by flow cytometry and WB. (**D, E**) The supernatant level of IL-1β and MCP-1 in HG-induced RAW 264.7 cells in the presence of MT or NAC ($n$=4). Data are provided as mean ± SEM. Statistically significant differences ($^{**}P<0.01$ vs. RAW 264.7 group; $^{\&}P<0.05$, $^{\&\&}P<0.01$ vs. HG group) are indicated.

transcription factor EB (TFEB) in the macrophages of diabetic mice (Figure 6D). In addition, comparing with the M2-like macrophages from diabetic mice, the LysoTracker-red intensity and protein levels of TFEB and CTSB in M1-like macrophages were significantly decreased, indicating the impaired lysosome in M1-like macrophages (Figure 6E,F). Based on the essential role of lysosome in autophagic flux, we measured the autophagic flux process using a tandem fluorescence RFP-GFP-LC3 reporter system, where autolysosome accumulation was indicated by RFP (red) and autophagosome abundance was indicated by dual fluorescence (GFP-RFP; yellow), and we found that the number of yellow dots in M1-like macrophages was increased (Figure 6G). Moreover, the protein level of P62 in M1-like macrophages was markedly increased (Figure 6E,F). These results demonstrated that diabetes impairs both lysosome function and autophagic flux during macrophage polarization.

*Clinical Science* (2019) **133** 1759–1777
https://doi.org/10.1042/CS20190672

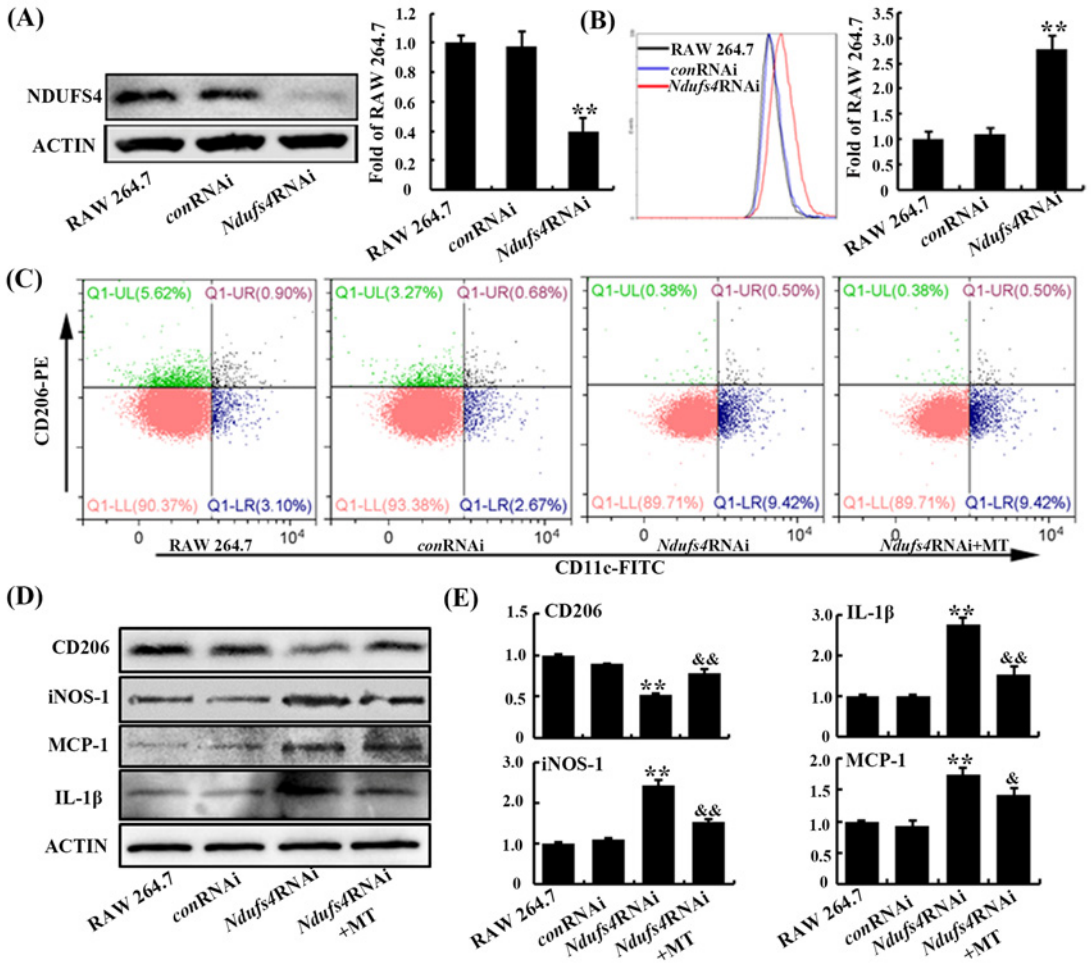


**Figure 5. Excessive accumulation of mitochondria ROS mediated by *Ndufs4*-RNAi promotes RAW 264.7 to polarize toward M1 phenotype**

(**A**) Expression of NDUFS4 in *Ndufs4*-RNAi RAW 264.7 cells ($n$=3). (**B**) Quality of mitochondrial ROS when the cells were transfected by *Ndufs4*-RNAi for 48 h by flow cytometry ($n$=4). (**C**) The analysis of polarized phenotype in *Ndufs4*RNAi RAW 264.7 cells with mitochondrial ROS inhibitor Mito-TEMPO (MT, 50 nM) ($n$=3). (**D, E**) Immunoblot quantification of inflammatory proteins and markers of polarized macrophages ($n$=4). Data are provided as mean ± SEM. Statistically significant differences (**$P$<0.01 vs. RAW 264.7 group; $^{\&}P$<0.05, $^{\&\&}P$<0.01 vs. *Ndufs4*-RNAi group) are indicated.

In line with the *in vivo* results, after the addition of a HG medium to RAW 264.7 cells the LC3II protein level was increased for the first 72 h and then reduced after 96 h of incubation (Figure 7A,B). In the presence of the lysosomal acidification inhibitor hydroxychloroquine (HCQ), the LC3II protein was dramatically elevated in normal macrophages but only slightly elevated in HG-stimulated macrophages (Figure 7C), suggesting that the autophagic flux is impaired under HG conditions. In term of the autophagic flux measured by RFP-GFP-LC3, HG treatment for 72 h increased the number of yellow dots per cell, while no significant change was observed when HCQ was added (Figure 7D). Additionally, an accumulation of ubiquitylated proteins was observed at 48 h (Figure 7E). These results demonstrated that autophagy is impaired under HG conditions. To determine the role of autophagy in M1 switching, autophagy was blocked using *Atg5*siRNA, or HCQ. Silencing *Atg5* in RAW 264.7 cells induced a decreased expression of ATG5 and an increased expression of P62. This is indicative of impaired autophagy. Consistently, impaired autophagy was associated with an increase in iNOS-1 expression in RAW 264.7 cells (Figure 7F). Similarly, HCQ treatment also promoted RAW 264.7 cell polarization into a pro-inflammatory phenotype (Figure 7G). These results demonstrated that autophagy impairment sufficiently induces M1 switching.

The essential proteins for recruitment of damaged mitochondria to autophagosomes, including PTEN-induced putative kinase 1 (PINK1) and PARKIN, were up-regulated in RAW 264.7 cells in a HG medium (Figure 8A,B). This

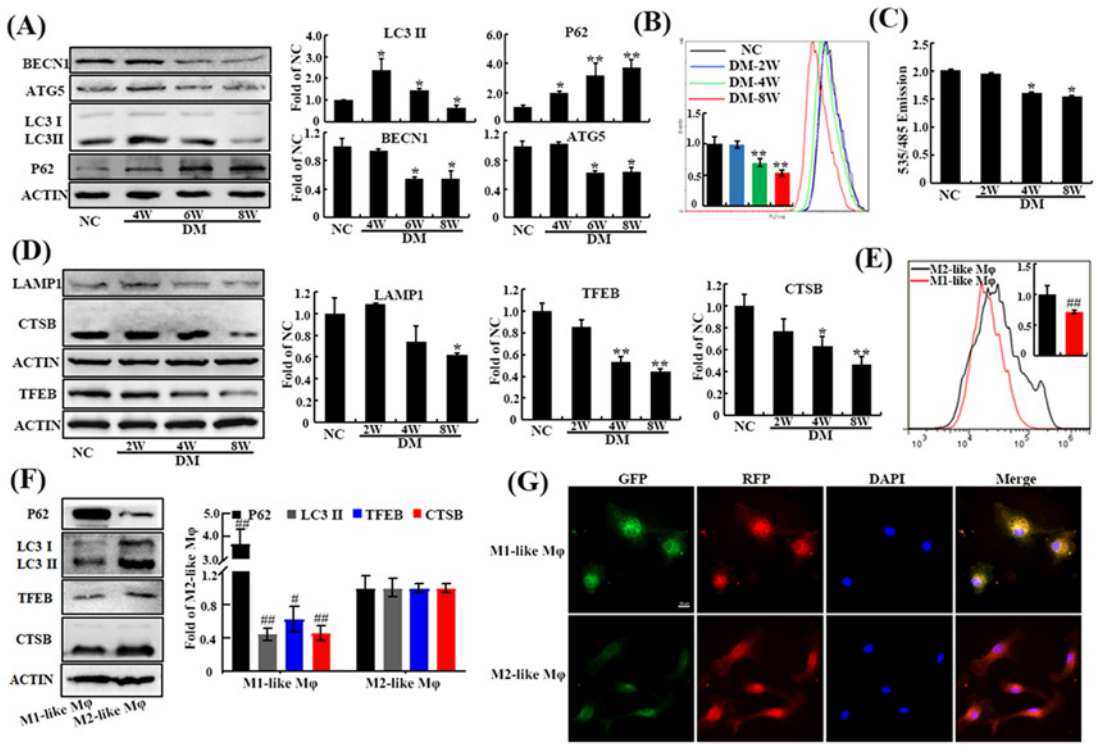


**Figure 6. Hyperglycemia induced macrophages lysosome dysfunction and impaired autophagy in diabetic mice**

Peritoneal macrophages were harvested by lavage from diabetic mice at 2, 4, 6, and 8 week post STZ injection. (**A**) Immunoblot of autophagy-related proteins (BECN1, ATG5, LC3, and P62) ($n$=4). (**B**) The quality of lysosome by LysoTracker-red probe (100 nM, 37°C for 30 min). (**C**) Measurement of lysosomal pH by LysoSensor Yellow/Blue (1 mg/ml, 37°C for 5 min), and the changes in pH were quantified as the ratio of emission 485/535 nm ($n$=4). (**D**) Expression of LAMP1, TFEB, and CTSB in macrophages ($n$=3). (**E**) The quality of lysosome in M1-like and M2-like macrophages (M1-like Mϕ and M2-like Mϕ; $n$=3). (**F**) Immunoblot of autophagy-related proteins (CTSB, TFEB, LC3, and P62) ($n$=3). (G) M1-like and M2-like macrophages were transduced with GFP-RFP-LC3 adenovirus for 24 h, and then cells were imaged via confocal microscopy. Scale bars: 10 μm. Data are provided as mean ± SEM. Statistically significant differences (*$P$<0.05, **$P$<0.01 vs. NC group; $^{\#}P$<0.05, $^{\#\#}P$<0.01 vs. M2-like Mϕ group) are indicated.

suggests that a HG environment might promote the formation of mitophagosomes. To further investigate the effect of a HG environment on mitophagy, we incubated RAW 264.7 cells with a HG medium or with CCCP (mitophagy inducer). CCCP enhanced the co-localization of Mito-Red with LC3, decreased the co-localization of Mito-Red with Lyso-Green, and reduced the mitochondrial proteins (TOM20 and TIM23) in RAW 264.7 cells. By contrast, incubation with HG- or HCQ-enriched medium enhanced mitochondria–lysosome co-localization (Figure 8C,D) and induced TOM20 and TIM23 protein expression in RAW 264.7 cells (Figure 8E). These results indicate that the clearance of damaged mitochondria in the lysosomes of macrophages is impaired as a response to a HG environment.

We next examined lysosomal proteolysis and lysosomal function in RAW 264.7 cells. Incubation of RAW 264.7 cells in HG medium for 48 h significantly increased the size of LAMP1$^{+}$ vesicles, and the diameter of lysosomes increased from a normal diameter of 0.4–0.5 to 0.82 ± 0.03 μm (Figure 9A,B). Similar to the primary macrophages from diabetic mice, a HG environment time-dependently inhibited LysoTracker intensity and elevated pH levels in RAW 264.7 cells (Figure 9C–F). The protein levels of CSTB and LAMP1 were significantly reduced after HG treatment (Figure 9G). The *Ndufs4* knockdown-induced mitochondrial respiratory dysfunction model showed reduced LysoTracker intensity, elevated lysosomal pH, and decreased levels of CTSB, TFEB, and LAMP1 in RAW 264.7 cells (Figure 10).

## Inhibition of mitochondrial ROS prevents the M1 polarization of macrophages by improving autophagic flux

Mito-TEMPO effectively reversed the abnormalities of lysosomes in HG-treated RAW 264.7 cells (Figure 9), suggesting that mitochondrial ROS cause lysosomal defects in diabetes. Moreover, Mito-TEMPO partly restored lysosomal

*Clinical Science* (2019) **133** 1759–1777
https://doi.org/10.1042/CS20190672

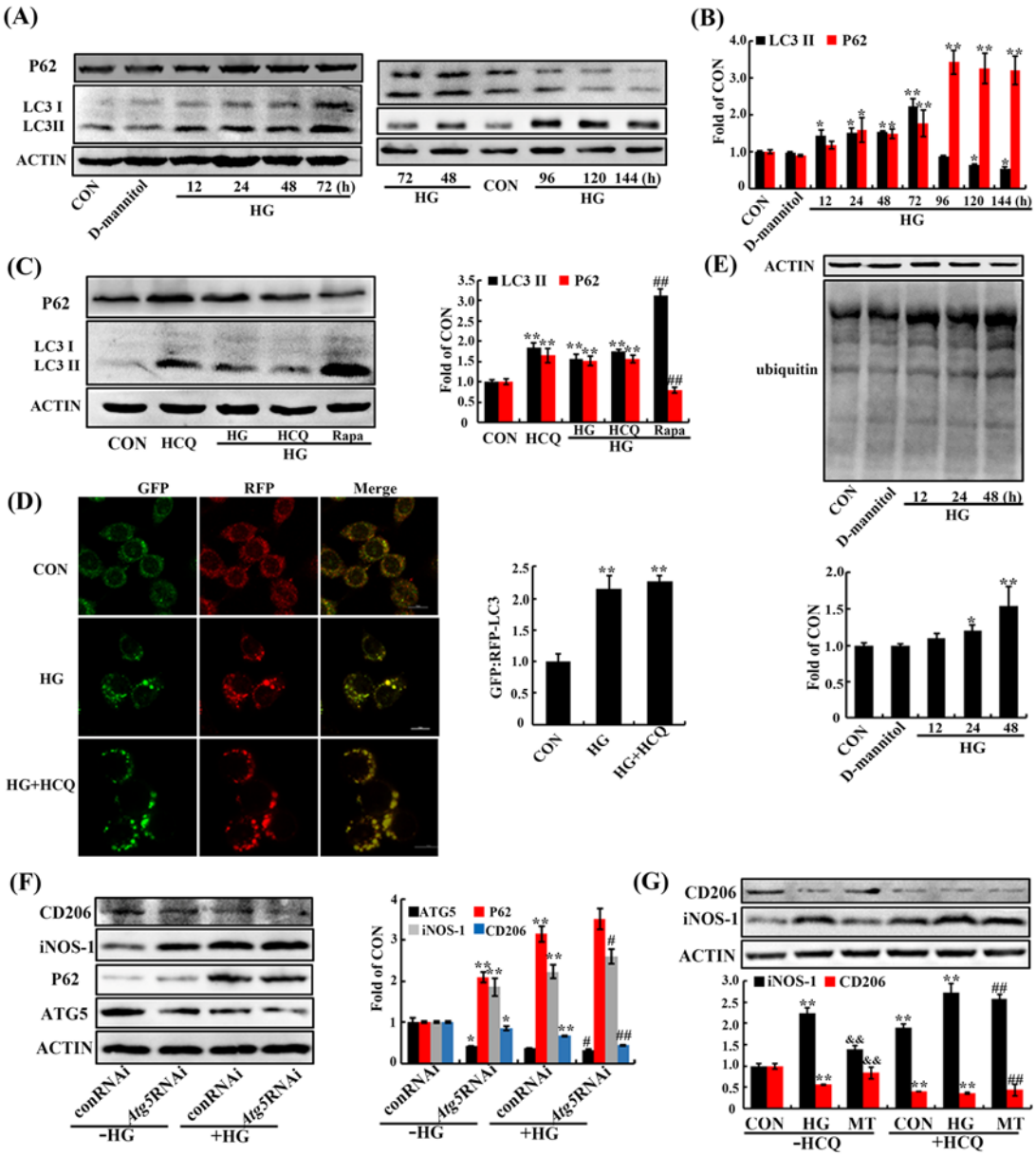


**Figure 7. HG induced autophagic flux blocked in RAW 264.7 cells**

(**A, B**) Immunoblot of LC3 and P62 in RAW 264.7 cells after the treatment of HG for different time ($n$=4). (**C**) The expression of P62 and LC3 in HG-induced RAW 264.7 cells with the treatment of hydroxychloroquine (HCQ, 20 μM, for the last 6 h) and rapamycin (Rapa, 100 nM). (**D**) Differentiated RAW264.7 cells were transduced with GFP-RFP-LC3 adenovirus for 24 h followed by exposure to HG for 48 h, and then cells were imaged via confocal microscopy. Scale bars: 10 μm. (**E**) The expression of ubiquitin in HG-induced RAW 264.7 cells. (**F, G**) Protein levels of CD206 and iNOS-1 in *Atg5*RNAi cells or HCQ-treated cells ($n$=4). Data are provided as mean ± SEM. Statistical significant differences ($^{*}P<0.05$, $^{**}P<0.01$ vs. CON group; $^{\#}P<0.05$, $^{\#\#}P<0.01$ vs. HG group; $^{\&\&}P<0.01$ vs. MT+HCQ group) are indicated.

intensity and function in *Ndufs4*-silenced RAW 264.7 cells (Figure 10A–D). These results indicated that mitochondrial ROS induces lysosomal disorder in macrophages.

Having shown that mitochondrial ROS impaired autophagic flux and lysosomal dysfunction during the M1 polarization of macrophages, we hypothesized that inhibition of mitochondrial ROS could prevent macrophage polarization to the M1 phenotype by improving autophagic flux. In support of this hypothesis, the effects of Mito-TEMPO on

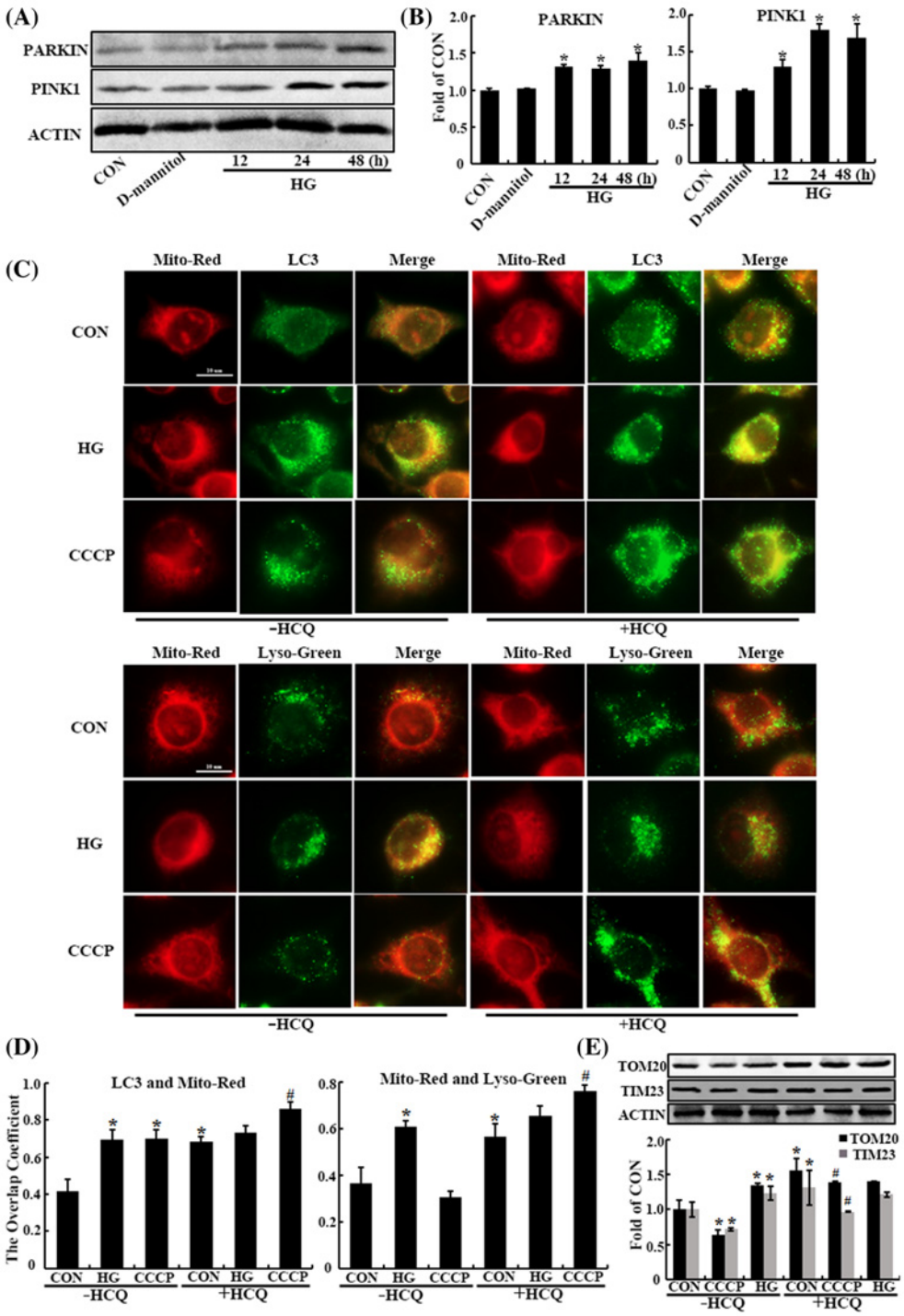


**Figure 8. HG inhibited the clearance of damaged mitochondrial in RAW 264.7 cells**

To induce mitophagy, RAW 264.7 cells were treated with CCCP (10 μM for 6h). (**A, B**) The expression of mitophagy-related proteins (PARKIN and PINK1) ($n$=4). (**C, D**) Co-localization of mitochondria with autophagosome marker LC3 or LysoTracker-green in HG-induced RAW 264.7 cells. (**E**) The expression of TOM20 and TIM23 in HG-induced RAW 264.7 cells ($n$=3). Data are provided as mean ± SEM. Statistically significant differences (*$P$<0.05; #$P$ <0.05 vs. CCCP group) are indicated.

*Clinical Science* (2019) **133** 1759–1777
https://doi.org/10.1042/CS20190672

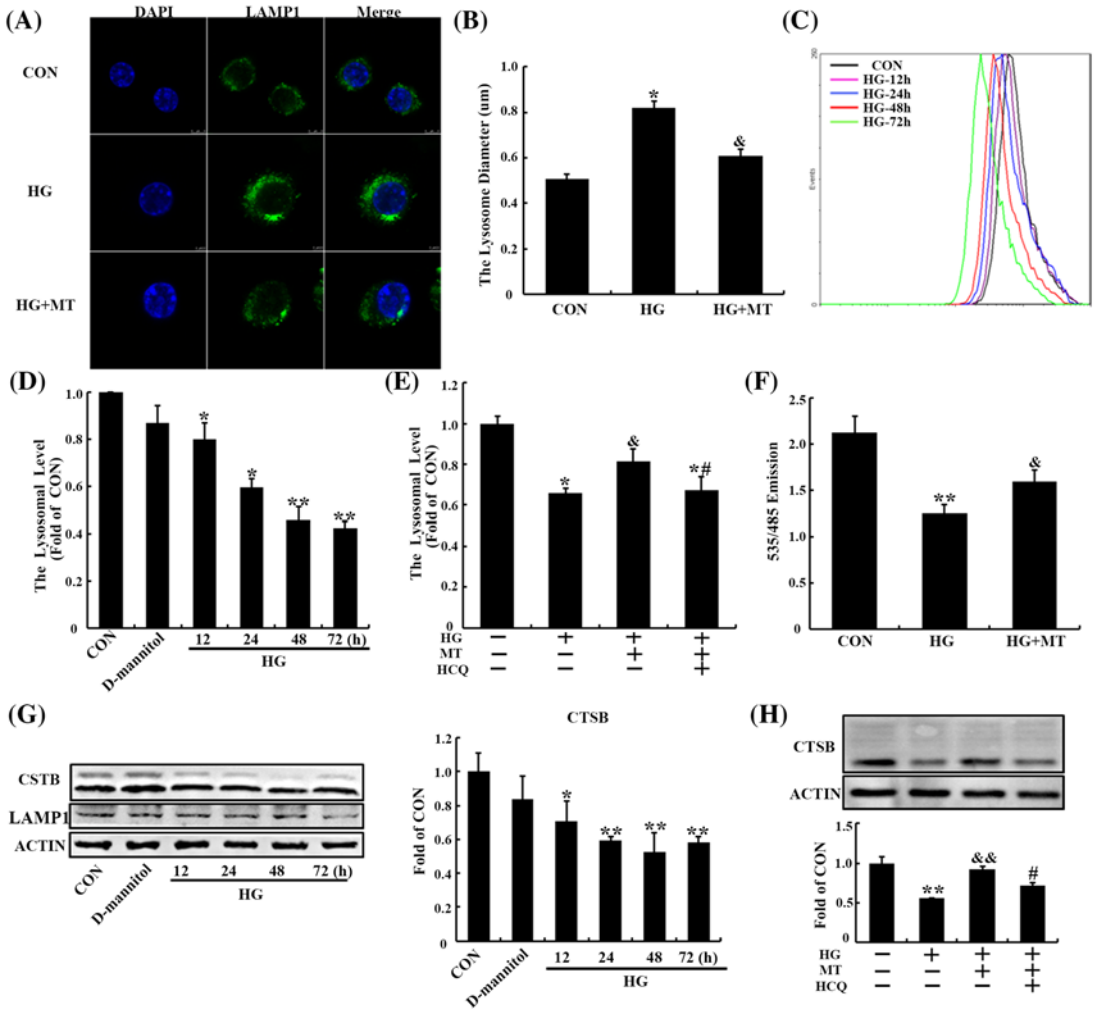


**Figure 9. HG impairs lysosomal function in RAW 264.7cells**

(**A, B**) Confocal microscopy of RAW 264.7 cells loaded with HG and stained with LAMP1 (lysosomal-associated membrane protein 1) antibody. Lysosome diameter was quantified from $n$=15 cells. (**C, D**) Quality of lysosome stained by lyso-tracker-red ($n$=4). (**E**) The effects of Mito-TEMPO (MT) or HCQ on lysosome ($n$=4). (**F**) Lysosomal pH level in HG-induced RAW 264.7 cells with MT or HCQ ($n$=3). (**G**) The expression of CTSB and LAMP1 in RAW 264.7 cells with HG for different time ($n$=3). (**H**) The expression of CTSB in RAW 264.7 cells with the treatment of Mito-TEMPO (MT) or HCQ ($n$=3). Data are provided as mean ± SEM. Statistically significant differences ($^{*}P<0.05$, $^{**}P<0.01$ vs. CON group; $^{\&}P<0.05$, $^{\&\&}P<0.01$ vs. HG; $^{\#}P<0.05$ vs. HG+MT group) are indicated.

the percentage of M1 macrophages, iNOS, and CD206 expression were partly reversed by co-incubation with HCQ (Figure 7G).

# Discussion

The major findings of the study are as follows: (1) the diabetic condition impaired mitochondrial function and lysosome-mediated autophagosome clearance in macrophages; (2) mitochondrial dysfunction mediated autophagic flux defect by damaging lysosomal function, which led to an accumulation of autophagosomes; and (3) selective inhibition of mitochondrial ROS improved lysosomal function and autophagic flux, thereby reversing the pro-inflammatory polarization of macrophages. Our study uncovered a novel mechanism by which mitochondrial dysfunction via ROS production promotes macrophage polarization toward the M1 phenotype by impairing autophagic flux under diabetic conditions (Figure 11).

Recently, metabolic cascades have been increasingly recognized as mediators of macrophage polarization. For sustained energy production, M1 macrophages relied on glycolysis whereas M2 cells relied on mitochondrial oxidative

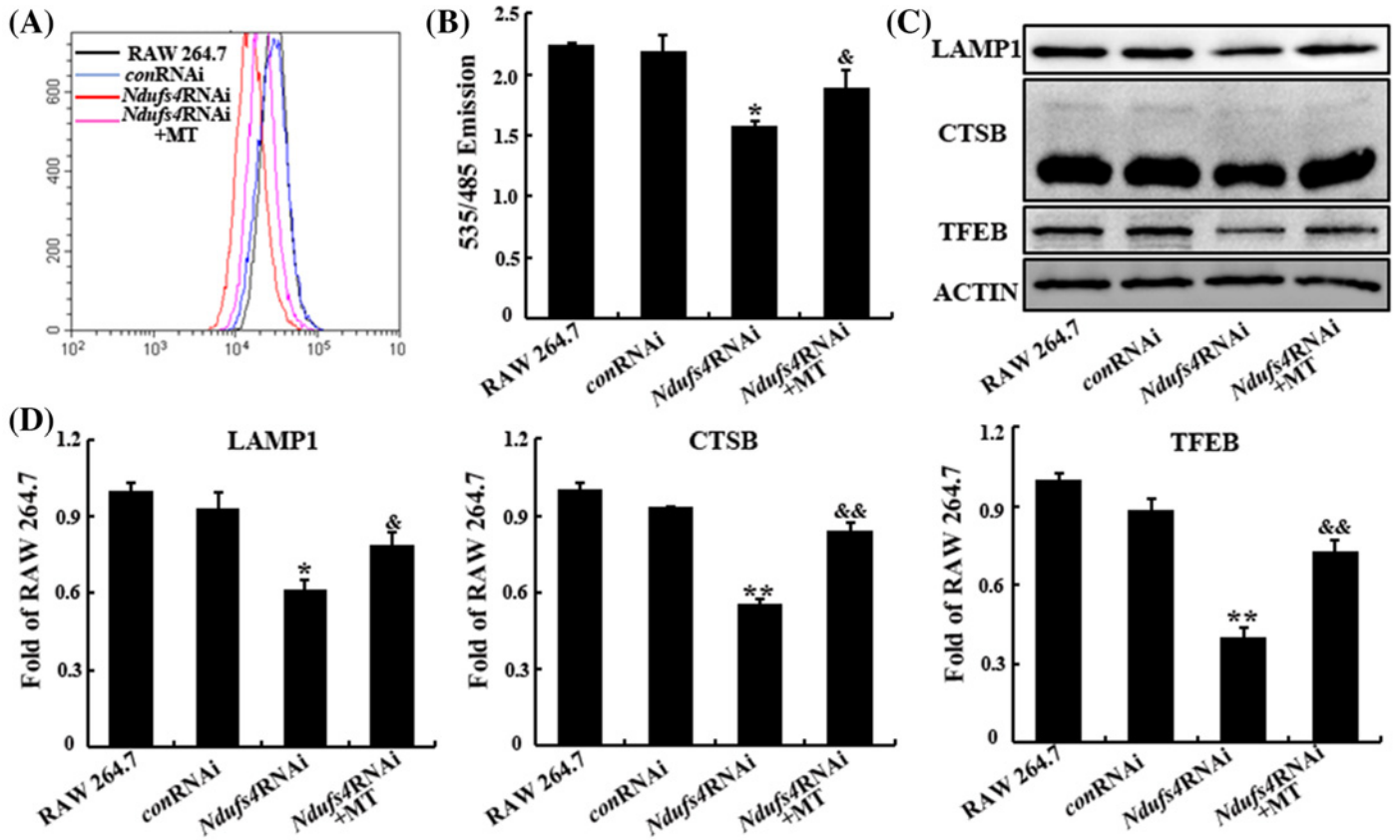


**Figure 10. Mitochondria dysfunction mediated by *Ndufs4*RNAi impairs lysosomal function in RAW 264.7 cells**

(**A**) The effects of *Ndufs4*RNAi and MT on lysosome quality analyzed by lyso-tracker-Red ($n$=3). (**B**) Lysosomal pH level in RAW 264.7 cells with mitochondrial dysfunction ($n$=4). (**C, D**) The expression of CTSB, TFEB and LAMP1 in RAW 264.7 cells ($n$=3). Data are provided as mean ± SEM. Statistically significant differences (*$P$<0.05, **$P$<0.01 vs. RAW 264.7 group; $^{\&}P$<0.05, $^{\&\&}P$<0.01 vs. *Ndufs4*RNAi group) are indicated.

phosphorylation (OXPHOS) [24,25]. Studies reported that ROS generation caused by mitochondrial dysfunction promoted NLRP3 inflammasome activation and other inflammatory responses in macrophages [26,27]. Contrarily, M1 macrophages induced by LPS + IFNγ exhibited mitochondrial dysfunction because of defective mitochondrial oxidative respiration. In addition, inhibiting nitric oxide (NO) production dampened the decline of mitochondrial OXPHOS in M1 macrophages to improve metabolic and phenotypic reprogramming to M2 macrophages [12]. Maintaining mitochondrial function was important for the reprogramming of M1 macrophages toward the M2 phenotype.

Mitochondria are highly dynamic organelles for the sustained balance of fission and fusion that undergo remodeling to meet the metabolic demands of the cell. Previous studies have shown that high glucose increased the protein expression and phosphorylation of DRP1, thus further leading to the translocation from cytoplasmic to the mitochondrial and increase in mitochondrial fission [28]. Moreover, DRP1 inhibitor mdivi-1, silencing of DRP1 or mutant of phosphorylation site could inhibit mitochondrial fission and improve biochemical and histological features of diabetic complications [29,30]. In our study, we demonstrated that the diabetic condition induces mitochondrial fission and excessive ROS production in macrophages. Furtherly, selective inhibition of mitochondrial ROS improves mitochondrial bioenergetics and inhibits DRP1-mediated mitochondrial fission, which results to the macrophage polarization from M1 to M2 under diabetic conditions. As a result, the presence of the mitochondrial-targeted antioxidant, Mito-TEMPO, prevents the release of HG-stimulated inflammatory cytokines such as MCP-1 in macrophages. Moreover, those cytokines have been recognized as key contributors to diabetic nephropathy [6]. Taken together, the mitochondrial ROS-mediated M1 polarization of macrophages and subsequent release of pro-inflammatory cytokines might represent an important mechanism contributing to diabetic complications [31]. This hypothesis was further supported by a recent study that reported that the administration of Mito-TEMPO reduced diabetic cardiomyopathy in mouse models of type-1 and type-2 diabetes [32].

*Clinical Science* (2019) **133** 1759–1777
https://doi.org/10.1042/CS20190672

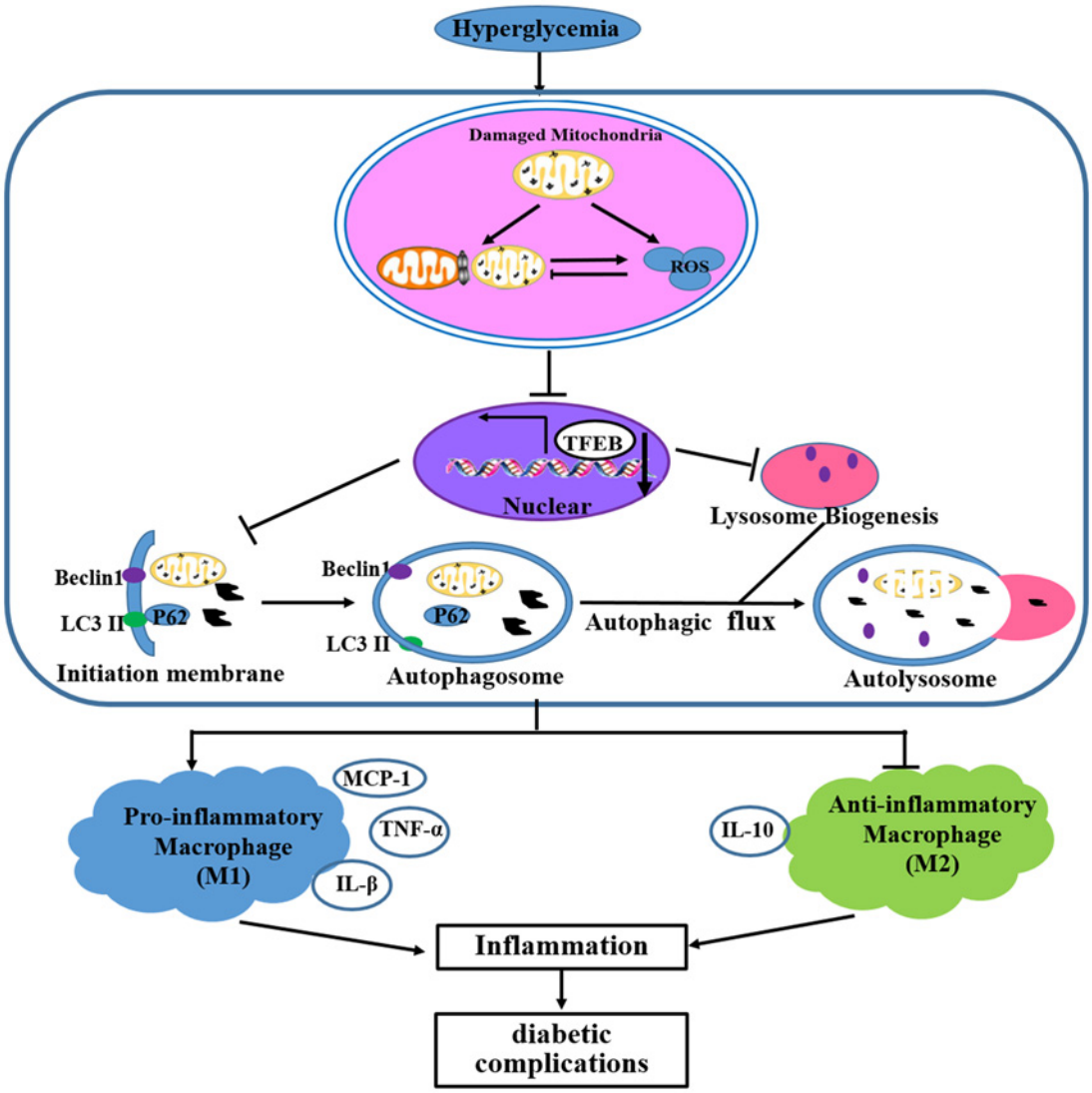


**Figure 11. Schematic representation of the regulatory role of mitochondria and autophagy–lysosome system in macrophages**

Under normal physiological conditions, damaged mitochondria was recognized and degradation in lysosome though autophagy process. However, under hyperglycemia condition, along with the massive accumulation of damaged mitochondria, the degradation capacity of lysosome was impaired. Besides, TFEB-mediated lysosome biogenesis in macrophages cells was decreased. As a result, the balance between macrophages polarization was disordered, leading to inflammatory phenotype in macrophages cells.

Mitochondrial dysfunction has been shown to compromise lysosome function and the autophagy process [22,23]. Our study extended this observation to macrophages. First, both diabetes and *Ndufs4*-RNAi induced mitochondrial dysfunction and impaired autophagosome clearance by disrupting lysosomal function, which led to increased levels of M1 macrophages and pro-inflammatory cytokines. Second, both autophagic flux and the maturation of autophagosomes, characterized as reduced LC3II and autophagosome-synthesis related protein (BECN 1 and ATG5), were impaired in the macrophages of diabetic mice. These data support a model that diabetes-induced mitochondrial ROS could impair lysosomal function and autophagic flux, thereby promoting M1 polarization and inflammatory cytokine release in macrophages.

However, the exact mechanism underlying mitochondrial dysfunction-induced lysosome impairment is incompletely understood. Recent studies found a critical role of TFEB in many processes in respect to enhanced autophagy and lysosomal function [33,34]. Notably, under conditions of lysosomal stress, TFEB is translocated to the nucleus

in several models of lysosomal storage disorders, initiating the expansion of the lysosomal compartment of the cell and the degradation of accumulated lysosomal contents [35]. It was also reported that the suppression of the mechanistic target of rapamycinm (mTOR) and the activation of calcineurin promoted TFEB nuclear translocation and thus enhanced autophagy and lysosome biogenesis and function in macrophages – all of which could ameliorate the lipid overload in atherosclerotic plaques [36,37]. In the present study, we showed that the expression of TFEB is decreased in macrophages starting 4 weeks after diabetes onset, which might explain the inhibition of autophagosome maturation in macrophages. On the other hand, BECN1 inhibition of TFEB activation was shown to decrease mitochondrial quality and cardiomyocyte death under stress by PGC-1$\alpha$-mediated mitochondrial biogenesis [38]. Additionally, PGC-1$\alpha$ induction ameliorated HD neurodegeneration and virtually eliminated Huntingtin (htt) protein aggregation by transactivation of TFEB [39]. These studies suggest a potential cross-talk between TFEB and PGC-1$\alpha$ in the regulation of lysosome and mitochondria function.

ROS were generated mainly as byproducts of mitochondrial respiration, and elevated ROS were highly associated with various metabolic and neurodegenerative diseases [40]. A recent study showed that elevated ROS levels triggered lysosome biogenesis and autophagy by calcineurin-dependent $Ca^{2+}$ release and nuclear translocation of TFEB [41]. These effects were abolished by *N*-acetylcysteine (NAC, a common antioxidant) [41]. Moreover, a similar observation was reported in THP-1 cells, in which autophagy was activated after treated with hypericin-mediated SDT (HY-SDT) for 6 h [42], suggests that ROS contribute to TFEB-mediated lysosome biogenesis and autophagy activation. In the present study, we proved that chronic HG-induced long-term ROS overload causes remarkable mitochondrial injury in macrophages, whereas scavenging mitochondrial ROS improves mitochondrial biogenesis and lysosomal function. It is well-known that a moderate increase in ROS may serve as a signal to trigger autophagy as a compensative mechanism. However, excessive accumulation of ROS may additionally cause severe oxidative damage to proteins and organelles in cells. A prior report demonstrated that acute mitochondrial stress, triggered by the AMPK-TFEB/MITF pathway, enhanced lysosomal biogenesis [42]; however, chronic mitochondrial stress led to the repression of lysosomal biogenesis [42]. Therefore, the long-term and excessive accumulation of mitochondrial ROS might lead to lysosomal dysfunction in macrophages in people with diabetes.

In summary, we have provided evidence to demonstrate that, under diabetic conditions, the loss of mitochondrial function results in ROS generation, which impairs lysosomes and blocks autophagic flux in macrophages. Defective autophagic flux further promotes macrophage polarization toward the M1 phenotype and produces low-grade inflammation. Thus, the present study significantly increases our understanding of the pathogenesis for diabetes and might offer potential therapy targets to prevent diabetic complications.

## Clinical perspectives

- Macrophage polarization toward the M1 phenotype and its subsequent inflammatory response have been implicated in the progression of diabetic complications, however, the mechanism involved in the regulation of macrophages polarization is incompletely understood.
- Our study uncovered a novel mechanism by which mitochondrial dysfunction via ROS production promotes macrophage polarization toward the M1 phenotype by impairing autophagic flux under diabetic conditions.
- These findings prove that mitochondrial ROS plays a key role in M1 macrophage polarization, which might provide clue to a novel treatment for diabetic complications.

### Acknowledgments

The authors would like to extend thanks to William Bresette in Arizona State University for his great proofreading.

### Funding

This work was supported by the National Natural Science Foundation of China [grant numbers 81370824 and 31571474]; and the China Postdoctoral Science Foundation [grant number 2017M620428].

*Clinical Science* (2019) **133** 1759–1777
https://doi.org/10.1042/CS20190672

## Author Contribution

The study was conceived by Yujia Yuan and Yanrong Lu, and developed by Jingping Liu and Jingqiu Cheng. Yujia Yuan performed the experiments and data collection with help from Lan Li, Wuzheng Zhu, Fei Liu, Shuyun Liu, Xingxing An, and Ruixi Luo. The paper was written by YujiaYuan and edited by Younan Chen and Tianqing Peng.

## Competing Interests

The authors declare that there are no competing interests associated with the manuscript.

## Abbreviations

ATG5, autophagy related 5; CTSB, cathepsin B; DM, diabetes mellitus; DRP1, dynamin-related protein 1; ER, endoplasmic reticulum; HCQ, hydroxychloroquine; HG, high glucose; HY-SDT, hypericin-mediated SDT; IL1β, interleukin-1β; IL6, interleukin-6; iNOS, inducible nitric oxide; LC3 II, microtubule-associated protein 1 light chain 3 II; MFN2, mitofusin-2; mTOR, mechanistic target of rapamycin; NAC, *N*-acetylcysteine; NC, normal control; NO, nitric oxide; OXPHOS, oxidative phosphorylation; PBS, phosphate buffered saline; PGC-1α, peroxisome proliferator-activated receptor gamma coactivator-1α; PINK1, PTEN induced putative kinase 1; PTCs, proximal tubular cells; RNS, reactive nitrogen species; ROS, reactive oxygen species; STZ, streptozotocin; TFEB, transcription factor EB; TNF-α, tumor necrosis factor α.

# References

1 Ogurtsova, K., da Rocha Fernandes, J.D., Huang, Y., Linnenkamp, U., Guariguata, L., Cho, N.H. et al. (2017) IDF diabetes atlas: global estimates for the prevalence of diabetes for 2015 and 2040. *Diabetes Res. Clin. Pract.* **128**, 40–50, https://doi.org/10.1016/j.diabres.2017.03.024
2 Gao, H.X., Regier, E.E. and Close, K.L. (2016) International Diabetes Federation World Diabetes Congress 2015. *J. Diabetes* **8**, 300–302, https://doi.org/10.1111/1753-0407.12377
3 Zheng, Z. and Zheng, F. (2016) Immune cells and inflammation in diabetic nephropathy. *J. Diabetes Res.* **2016**, 1841690
4 Asghar, A. and Sheikh, N. (2017) Role of immune cells in obesity induced low grade inflammation and insulin resistance. *Cell. Immunol.* **315**, 18–26, https://doi.org/10.1016/j.cellimm.2017.03.001
5 Niu, S., Bian, Z., Tremblay, A., Luo, Y., Kidder, K., Mansour, A. et al. (2016) Broad infiltration of macrophages leads to a proinflammatory state in streptozotocin-induced hyperglycemic mice. *J. Immunol.* **197**, 3293–3301, https://doi.org/10.4049/jimmunol.1502494
6 Awad, A.S, You, H., Gao, T., Cooper, T.K., Nedospasov, S.A., Vacher, J. et al. (2015) Macrophage-derived tumor necrosis factor-alpha mediates diabetic renal injury. *Kidney Int.* **88**, 722–733, https://doi.org/10.1038/ki.2015.162
7 Tian, S. and Chen, S.Y. (2015) Macrophage polarization in kidney diseases. *Macrophage* **2**, pii: e679, https://doi.org/10.14880/macrophage.679
8 Wang, X., Yao, B., Wang, Y., Fan, X., Wang, S., Niu, A. et al. (2017) Macrophage cyclooxygenase-2 protects against development of diabetic nephropathy. *Diabetes* **66**, 494–504, https://doi.org/10.2337/db16-0773
9 Torres-Castro, I., Arroyo-Camarena, U.D., Martinez-Reyes, C.P., Gomez-Arauz, A.Y., Duenas-Andrade, Y., Hernandez-Ruiz, J. et al. (2016) Human monocytes and macrophages undergo M1-type inflammatory polarization in response to high levels of glucose. *Immunol. Lett.* **176**, 81–89, https://doi.org/10.1016/j.imlet.2016.06.001
10 Padgett, L.E., Burg, A.R., Lei, W. and Tse, H.M. (2015) Loss of NADPH oxidase-derived superoxide skews macrophage phenotypes to delay type 1 diabetes. *Diabetes* **64**, 937–946, https://doi.org/10.2337/db14-0929
11 Tan, H.Y., Wang, N., Li, S., Hong, M., Wang, X. and Feng, Y. (2016) The reactive oxygen species in macrophage polarization: reflecting its dual role in progression and treatment of human diseases. *Oxid. Med. Cell Longev.* **2016**, 2795090, https://doi.org/10.1155/2016/2795090
12 Van den Bossche, J., Baardman, J., Otto, N.A., van der Velden, S., Neele, A.E., van den Berg, S.M. et al. (2016) Mitochondrial dysfunction prevents repolarization of inflammatory macrophages. *Cell Rep.* **17**, 684–696, https://doi.org/10.1016/j.celrep.2016.09.008
13 Kumar, P., Swain, M.M. and Pal, A. (2016) Hyperglycemia-induced inflammation caused down-regulation of 8-oxoG-DNA glycosylase levels in murine macrophages is mediated by oxidative-nitrosative stress-dependent pathways. *Int. J. Biochem. Cell Biol.* **73**, 82–98, https://doi.org/10.1016/j.biocel.2016.02.006
14 Jin, Z., Wei, W., Yang, M., Du, Y. and Wan, Y. (2014) Mitochondrial complex I activity suppresses inflammation and enhances bone resorption by shifting macrophage-osteoclast polarization. *Cell Metab.* **20**, 483–498, https://doi.org/10.1016/j.cmet.2014.07.011
15 Galluzzi, L., Baehrecke, E.H., Ballabio, A., Boya, P., Bravo-San Pedro, J.M., Cecconi, F. et al. (2017) Molecular definitions of autophagy and related processes. *EMBO J.* **36**, 1811–1836, https://doi.org/10.15252/embj.201796697
16 Ilyas, G., Zhao, E., Liu, K., Lin, Y., Tesfa, L., Tanaka, K.E. et al. (2016) Macrophage autophagy limits acute toxic liver injury in mice through down regulation of interleukin-1β. *J. Hepatol.* **64**, 118–127, https://doi.org/10.1016/j.jhep.2015.08.019
17 Liu, K., Zhao, E., Ilyas, G., Lalazar, G., Lin, Y., Haseeb, M. et al. (2015) Impaired macrophage autophagy increases the immune response in obese mice by promoting proinflammatory macrophage polarization. *Autophagy* **11**, 271–284, https://doi.org/10.1080/15548627.2015.1009787
18 Xi, X. and Ren, J. (2015) Macrophage migration inhibitory factor (MIF) knockout preserves cardiac homeostasis through alleviating Akt-mediated myocardial autophagy suppression in high-fat diet-induced obesity. *Int. J. Obes.* **39**, 387–396, https://doi.org/10.1038/ijo.2014.174
19 Yamamoto, T., Takabatake, Y., Takahashi, A., Kimura, T., Namba, T., Matsuda, J. et al. (2017) High-fat diet-induced lysosomal dysfunction and impaired autophagic flux contribute to lipotoxicity in the kidney. *J. Am. Soc. Nephrol.* **28**, 1534–1551, https://doi.org/10.1681/ASN.2016070731
20 Peres, G.B., Juliano, M.A., Aguiar, J.A. and Michelacci, Y.M. (2014) Streptozotocin-induced diabetes mellitus affects lysosomal enzymes in rat liver. *Braz. J. Med. Biol. Res.* **47**, 452–460, https://doi.org/10.1590/1414-431X20143386

21 Jung, M., Lee, J., Seo, H.Y., Lim, J.S. and Kim, E.K. (2015) Cathepsin inhibition-induced lysosomal dysfunction enhances pancreatic beta-cell apoptosis in high glucose. *PLoS One* **10**, e0116972, https://doi.org/10.1371/journal.pone.0116972
22 Baixauli, F., Acin-Perez, R., Villarroya-Beltri, C., Mazzeo, C., Nunez-Andrade, N., Gabande-Rodriguez, E. et al. (2015) Mitochondrial respiration controls lysosomal function during inflammatory T cell responses. *Cell Metab.* **22**, 485–498, https://doi.org/10.1016/j.cmet.2015.07.020
23 Demers-Lamarche, J., Guillebaud, G., Tlili, M., Todkar, K., Belanger, N., Grondin, M. et al. (2016) Loss of mitochondrial function impairs lysosomes. *J. Biol. Chem.* **291**, 10263–10276, https://doi.org/10.1074/jbc.M115.695825
24 Blagih, J. and Jones, R.G. (2015) Polarizing macrophages through reprogramming of glucose metabolism. *Cell Metab.* **15**, 793–795, https://doi.org/10.1016/j.cmet.2012.05.008
25 He, C. and Carter, A.B. (2015) The metabolic prospective and redox regulation of macrophage polarization. *J. Clin. Cell Immunol.* **6**, https://doi.org/10.4172/2155-9899.1000371
26 Park, S., Won, J.H., Hwang, I., Hong, S., Lee, H.K. and Yu, J.W. (2015) Defective mitochondrial fission augments NLRP3 inflammasome activation. *Sci. Rep.* **5**, 15489, https://doi.org/10.1038/srep15489
27 Carlos, D., Costa, F.R., Pereira, C.A., Rocha, F.A., Yaochite, J.N., Oliveira, G.G. et al. (2017) Mitochondrial DNA activates the NLRP3 inflammasome and predisposes to Type 1 diabetes in murine model. *Front. Immunol.* **8**, 164, https://doi.org/10.3389/fimmu.2017.00164
28 Wada, J. and Nakatsuka, A. (2016) Mitochondrial dynamics and mitochondrial dysfunction in diabetes. *Acta Med. Okayama* **70**, 151–158
29 Williams, M. and Caino, M.C. (2018) Mitochondrial dynamics in Type 2 diabetes and cancer. *Front. Endocrinol.* **9**, 211, https://doi.org/10.3389/fendo.2018.00211
30 Galvan, D.L., Long, J., Green, N., Chang, B.H., Lin, J.S., Schumacker, P. et al. Drp1S600 phosphorylation regulates mitochondrial fission and progression of nephropathy in diabetic mice. *J. Clin. Invest.* **130**, 127277
31 Navarro-Gonzalez, J.F., Mora-Fernandez, C., Muros de Fuentes, M., Chahin, J., Mendez, M.L., Gallego, E. et al. (2015) Effect of pentoxifylline on renal function and urinary albumin excretion in patients with diabetic kidney disease: the PREDIAN trial. *J. Am. Soc. Nephrol.* **26**, 220–229, https://doi.org/10.1681/ASN.2014010012
32 Ni, R., Cao, T., Xiong, S., Ma, J., Fan, G.C., Lacefield, J.C. et al. (2016) Therapeutic inhibition of mitochondrial reactive oxygen species with mito-TEMPO reduces diabetic cardiomyopathy. *Free Radic. Biol. Med.* **90**, 12–23, https://doi.org/10.1016/j.freeradbiomed.2015.11.013
33 Palmieri, M., Pal, R., Nelvagal, H.R., Lotfi, P., Stinnett, G.R., Seymour, M.L. et al. (2017) mTORC1-independent TFEB activation via Akt inhibition promotes cellular clearance in neurodegenerative storage diseases. *Nat. Commun.* **8**, 14338, https://doi.org/10.1038/ncomms14338
34 Moruno-Manchon, J.F., Uzor, N.E., Kesler, S.R., Wefel, J.S., Townley, D.M., Nagaraja, A.S. et al. (2016) TFEB ameliorates the impairment of the autophagy-lysosome pathway in neurons induced by doxorubicin. *Aging* **8**, 3507–3519, https://doi.org/10.18632/aging.101144
35 Raben, N. and Puertollano, R. (2016) TFEB and TFE3: linking lysosomes to cellular adaptation to stress. *Annu. Rev. Cell Dev. Biol.* **32**, 255–278, https://doi.org/10.1146/annurev-cellbio-111315-125407
36 Emanuel, R, Sergin, I., Bhattacharya, S., Turner, J., Epelman, S., Settembre, C. et al. (2014) Induction of lysosomal biogenesis in atherosclerotic macrophages can rescue lipid-induced lysosomal dysfunction and downstream sequelae. *Arterioscler. Thromb. Vasc. Biol.* **34**, 1942–1952, https://doi.org/10.1161/ATVBAHA.114.303342
37 Sergin, I., Evans, T.D., Zhang, X., Bhattacharya, S., Stokes, C.J., Song, E. et al. (2017) Exploiting macrophage autophagy-lysosomal biogenesis as a therapy for atherosclerosis. *Nat. Commun.* **8**, 15750, https://doi.org/10.1038/ncomms15750
38 Ma, X., Liu, H., Murphy, J.T., Foyil, S.R., Godar, R.J., Abuirqeba, H. et al. (2015) Regulation of the transcription factor EB-PGC1alpha axis by beclin-1 controls mitochondrial quality and cardiomyocyte death under stress. *Mol. Cell. Biol.* **35**, 956–976, https://doi.org/10.1128/MCB.01091-14
39 Tsunemi, T., Ashe, T.D., Morrison, B.E., Soriano, K.R., Au, J., Roque, R.A. et al. (2012) PGC-1$\alpha$ rescues Huntington's disease proteotoxicity by preventing oxidative stress and promoting TFEB function. *Sci. Transl. Med.* **4**, 142ra97, https://doi.org/10.1126/scitranslmed.3003799
40 Scherz-Shouval, R. and Elazar, Z. (2011) Regulation of autophagy by ROS: physiology and pathology. *Trends Biochem. Sci.* **36**, 30–38, https://doi.org/10.1016/j.tibs.2010.07.007
41 Zhang, X., Cheng, X., Yu, L., Yang, J., Calvo, R., Patnaik, S. et al. (2016) MCOLN1 is a ROS sensor in lysosomes that regulates autophagy. *Nat. Commun.* **30**, 12109, https://doi.org/10.1038/ncomms12109
42 Li, X., Zhang, X., Zheng, L., Kou, J., Zhong, Z., Jiang, Y. et al. (2016) Hypericin-mediated sonodynamic therapy induces autophagy and decreases lipids in THP-1 macrophage by promoting ROS-dependent nuclear translocation of TFEB. *Cell Death Dis.* **7**, e2527, https://doi.org/10.1038/cddis.2016.433

# Fig. S1

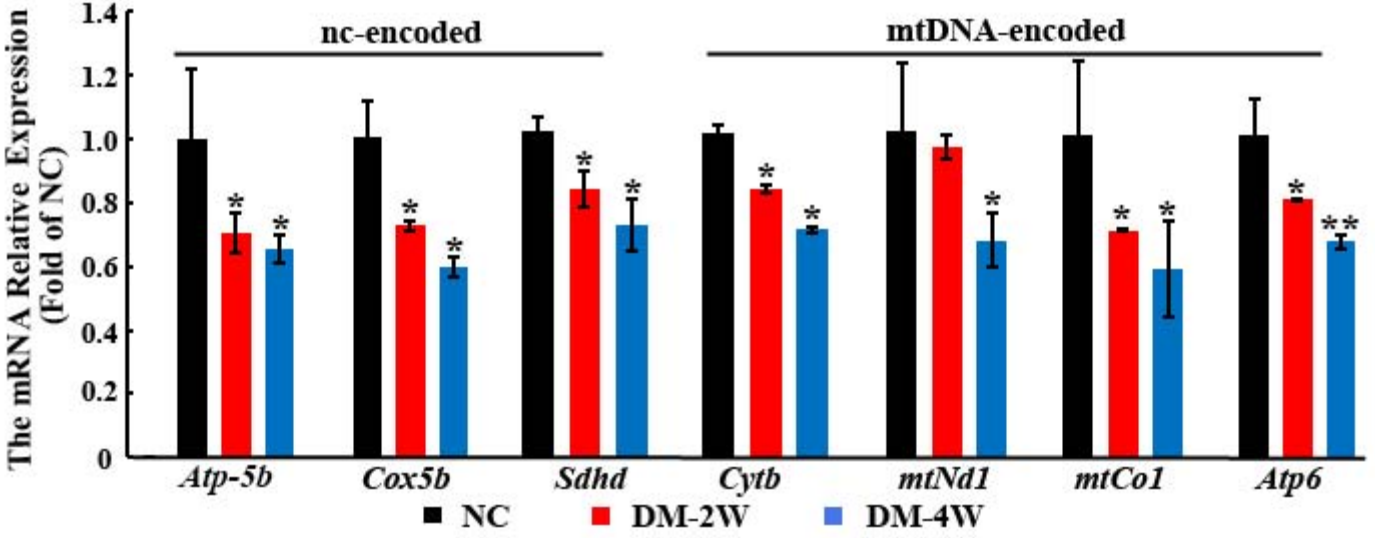
nc-encoded
mtDNA-encoded
The mRNA Relative Expression (Fold of NC)
1.4
1.2
1.0
0.8
0.6
0.4
0.2
0
Atp-5b
Cox5b
Sdhd
Cytb
mtNd1
mtCo1
Atp6
NC
DM-2W
DM-4W

# Fig. S2

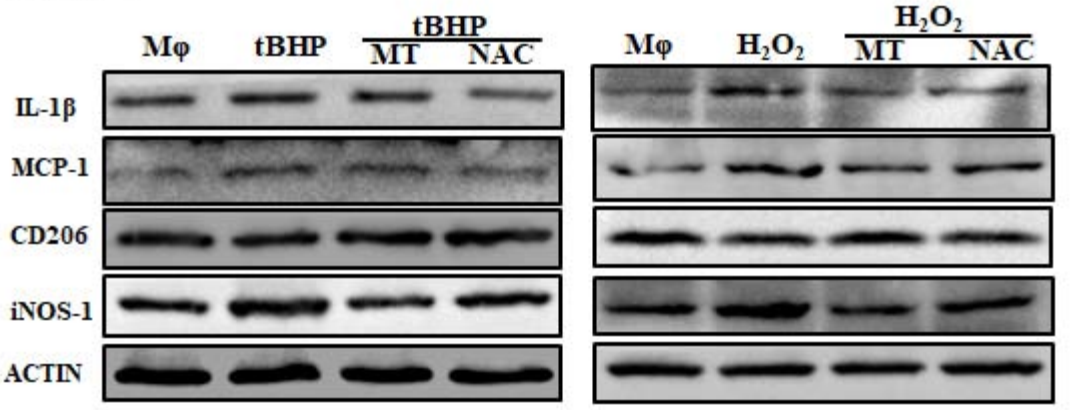
Mφ
tBHP
tBHP
MT
NAC
IL-1β
MCP-1
CD206
iNOS-1
ACTIN
Mφ
H2O2
H2O2
MT
NAC

**Table 1. Primers used for qPCR analysis**

| | | | |
|---|---|---|---|
| iNOS-F | CAGCTGGGCTGTACAAACCTT | ND1-F | CAAACCTCCTATCAGCCATCC |
| iNOS-R | CATTGGAAGTGAAGCGTTTCG | ND1-R | AGCGAAGAATCGGGTCAAG |
| Arg-1-F | AGACAGCAGAGGAGGTGAAGAG | CO1-F | TCTAATCGCCATAGCCTTCC |
| Arg-1-R | CGAAGCAAGCCAAGGTTAAAGC | CO1-R | GCGTCTGCAAATGGTTGTAA |
| CD206-F | GGATTGTGGAGCAGATGGAAG | ATP6-F | CTCACTTGCCCACTTCCTTC |
| CD206-R | CTTGAATGGAAATGCACAGA | ATP6-R | GTAAGCCGGACTGCTAATGC |
| ATP5B-F | TTTGCTGGTGTTGGTGAGAG | Cytb -F | CAAACCTCCTATCAGCCATCC |
| ATP5B-R | GGTGGTTCGTTCATCTGTCC | Cytb -R | AGCGAAGAATCGGGTCAAG |
| COX5b-F | CAGAAGGGACTGGACCCATA | ACTIN-F | AAGGCCAACCGTGAAAAGAT |
| COX5b-R | TTCACAGATGCAGCCCACTA | ACTIN-R | GTGGTACGACCAGAGGCATAC |
| SDHD-F | TGTCACCAAGCCACCACTC | | |
| SDHD-R | CCACAGAGCAGGGATTCAAG | | |